



Deposited via The University of Leeds.

White Rose Research Online URL for this paper:

<https://eprints.whiterose.ac.uk/id/eprint/131019/>

Version: Accepted Version

Article:

Magnall, JM, Gleeson, SA, Poulton, SW et al. (2018) Links between seawater paleoredox and the formation of sediment-hosted massive sulphide (SHMS) deposits — Fe speciation and Mo isotope constraints from Late Devonian mudstones. *Chemical Geology*, 490. pp. 45-60. ISSN: 0009-2541

<https://doi.org/10.1016/j.chemgeo.2018.05.005>

© 2018 Elsevier B.V. This manuscript version is made available under the CC-BY-NC-ND 4.0 license <http://creativecommons.org/licenses/by-nc-nd/4.0/>

Reuse

This article is distributed under the terms of the Creative Commons Attribution-NonCommercial-NoDerivs (CC BY-NC-ND) licence. This licence only allows you to download this work and share it with others as long as you credit the authors, but you can't change the article in any way or use it commercially. More information and the full terms of the licence here: <https://creativecommons.org/licenses/>

Takedown

If you consider content in White Rose Research Online to be in breach of UK law, please notify us by emailing eprints@whiterose.ac.uk including the URL of the record and the reason for the withdrawal request.

1
2
3
4
5 1 Links between seawater paleoredox and the formation of
6
7
8 2 sediment-hosted massive sulphide (SHMS) deposits – Fe
9
10
11
12 3 speciation and Mo isotope constraints from Late Devonian
13
14
15
16 4 mudstones

17
18
19 5 **Joseph M. Magnall¹, Sarah A. Gleeson^{1,2}, Simon W. Poulton³, Gwyneth G. Gordon⁴,**
20
21 6 **and Suzanne Paradis⁵**

22
23 7 ¹ *GFZ German Research Centre for Geosciences, 14473 Potsdam, Germany*

24
25 8 ² *Institute of Geological Sciences, Freie Universität Berlin, Malteserstrasse, 74-100, Berlin, 12249, Germany*

26
27 9 ³ *School of Earth and Environment, University of Leeds, Leeds, LS2 9JT, UK*

28
29 10 ⁴ *School of Earth and Space Exploration, Arizona State University, Tempe, AZ 85287, United States*

30
31 11 ⁵ *Geological Survey of Canada, Box 6000, 9860 West Saanich Road, Sidney, British Columbia, V8L 4B2, Canada*

32
33 12 **ABSTRACT**

34
35 13 Many models of sediment hosted massive sulphide (SHMS) deposit formation invoke
36
37 14 basin restriction events that resulted in long-term stagnation and anoxia, in which sulphidic
38
39 15 (euxinic) conditions ultimately prevailed. Euxinic conditions are then thought to provide a
40
41 16 chemical trap for hydrothermally exhaled base metals. Here, we present Fe speciation and Mo
42
43 17 isotope data for organic-rich mudstones from two drill-holes intersecting Upper Devonian strata,
44
45 18 deposited along the passive margin of ancestral North America. One drill-hole intersects a 35 m
46
47 19 thick sequence of SHMS mineralisation, while the other intersects correlative, un-mineralised
48
49 20 strata. All samples have high Fe_{HR}/Fe_T values (>0.38), indicating water-column anoxia. For the
50
51 21 majority of samples in the un-mineralised drill-hole, the levels of pyritisation fall below the
52
53 22 threshold typically used to define euxinic conditions ($Fe_{PY}/Fe_{HR} \leq 0.7$). In contrast, higher levels
54
55 23 of pyritisation in the mineralised drill-hole (median $Fe_{PY}/Fe_{HR} = 0.86$) likely developed via
56
57 24 diagenetic pyrite enrichment. Whereas Pb and Zn are negatively correlated with Mo, Mo-U co-
58
59
60
61
62
63
64
65

1
2
3
4 25 variation is consistent with Fe (oxyhydr)oxide particulate shuttling in the water-column. In
5
6 26 addition, a weak correlation between TOC/P and Mo provides further evidence that Mo was
7
8 27 sourced via authigenic, rather than hydrothermal, processes. The $\delta^{98}\text{Mo}$ values (+0.35 to +0.71‰)
9
10 28 are uniform between both drill-holes, and substantially lower than constraints for Late Devonian
11
12 29 seawater (+1.5 to +2.0‰), consistent with Mo adsorption to Fe (oxyhydr)oxides. Collectively, the
13
14 30 data provide evidence that local seawater was dominantly ferruginous (anoxic, non-sulphidic) at
15
16 31 Macmillan Pass. Regional variability in the extent of ferruginous (low TOC/P) and euxinic (high
17
18 32 TOC/P) conditions likely contributed to a balance between P regeneration and P enrichment that
19
20 33 maintained nutrient availability and productivity in the Selwyn Basin during the Late Devonian.
21
22 34 We argue that high primary productivity and enhanced organic carbon burial are key variables for
23
24 35 promoting sulphate reduction in the sub-surface. Moreover, how such conditions are maintained
25
26 36 over long periods of basin evolution is more important for producing effective metal traps in
27
28 37 SHMS systems, rather than a specific, localised redox condition of seawater (i.e. euxinia).
29
30
31
32
33
34

35
36
37
38
39
40
41
42
43
44
45
46
47
48
49
50
51
52
53
54
55
56
57
58
59
60
61
62
63
64
65

39 INTRODUCTION

40 Sediment-hosted massive sulphide (SHMS) deposits represent the anomalous enrichment
41 of reduced sulphur and base metals (Pb, Zn, Fe) within organic-rich marine strata (Ohmoto and
42 Goldhaber, 1997). A major challenge for previous studies on SHMS deposits has been to
43 determine the nature of the relationship between ambient paleoredox conditions and
44 mineralisation. Many deposits contain bedded (stratiform) sulphide mineralisation, which has led
45 to the development of sedimentary exhalative (SEDEX) models involving sulphide precipitation
46 from a stagnant water-column, where anoxic, sulphidic conditions (dissolved $\text{H}_2\text{S} > \text{Fe}^{2+}$; euxinic)
47 develop in restricted marine sub-basins (Goodfellow et al., 1993). Indeed, the development of
48 euxinic conditions has been proposed as the chemical trap for hydrothermally exhaled base
49 metals, and also provides a key component in the explanation for the secular distribution of
50 SHMS deposits within the geologic record (Goodfellow, 1987; Lyons et al., 2006; Turner, 1992).

1
2
3
4 51 Ultimately, this euxinic basin paradigm forms a framework for how basin architecture (i.e.
5
6 52 restriction) and geochemistry (i.e. stagnation, euxinia) is interpreted in SHMS systems, which
7
8 53 informs exploration models and the targeting of new discoveries.
9

10
11 54 Combining the iron and Mo based redox proxies can provide an important framework for
12
13 55 evaluating seawater paleoredox across different scales, both local and global (Scott and Lyons,
14
15 56 2012). Molybdenum is the most abundant transition metal in seawater, and is homogenously
16
17 57 distributed within the modern oceans ($\sim 8 \times 10^5$ yr residence time; Emerson and Huested, 1991).
18
19 58 Importantly, adsorption of Mo to Fe-Mn (oxyhydr)oxides in oxic seawater results in a large
20
21 59 isotopic fractionation, leading to modern seawater with a high $\delta^{98}\text{Mo}$ value (+2.4‰; Barling et
22
23 60 al., 2001; Barling and Anbar, 2004; Poulson et al., 2006; Siebert et al., 2003). In contrast, there is
24
25 61 minimal isotopic fractionation between seawater and sediments deposited under strongly euxinic
26
27 62 conditions in which H_2S concentrations exceed $11 \mu\text{M}$ (Erickson and Helz, 2000; Nägler et al.,
28
29 63 2005; Neubert et al., 2008). Assuming invariant Mo input to the oceans, periods of Earth history
30
31 64 with expanded euxinia are therefore characterised by $\delta^{98}\text{Mo}$ values that are lower relative to
32
33 65 modern oceans (e.g. Arnold et al., 2004). However, accurate interpretations require independent
34
35 66 constraints of local depositional redox conditions, and the need to specifically demonstrate the
36
37 67 occurrence of strongly euxinic conditions in which no fractionation occurs between seawater and
38
39 68 sediment (e.g. Gordon et al., 2009). This is typically achieved by the combined interpretation of
40
41 69 Mo and Fe geochemistry (Scott and Lyons, 2012), with the latter involving an evaluation of
42
43 70 sediment Fe enrichments and the degree to which Fe occurs within pyrite relative to other phases
44
45 71 containing reactive Fe (e.g. carbonate and oxide phases; Poulton and Canfield, 2005).
46
47
48
49
50

51 72 Despite the proposed link between seawater paleoredox and sulphide mineralisation, a
52
53 73 combined approach using Mo and Fe geochemistry has not yet been attempted on the organic-rich
54
55 74 mudstones that host SHMS deposits. In this study, we focus on Upper Devonian organic-rich
56
57 75 mudstones from the Selwyn Basin which, like other sedimentary basins of this age, is host to fine-
58
59 76 grained siliciclastic rocks deposited along the continental margin of ancestral North America
60
61
62
63
64
65

1
2
3
4 77 (Fig. 1). Unlike other Late Devonian basins of North America, the Selwyn Basin also hosts
5
6 78 SHMS mineralisation (Fig. 2A, B). At Macmillan Pass, two SHMS deposits occur within
7
8 79 Frasnian strata (Fig. 2C), where the full deposit architectures are well-preserved, comprising a
9
10 80 discrete feeder zone of massive sulphide and iron carbonate mineralisation overlain by a laterally
11
12 81 extensive sequence (hundreds of meters) of bedded sulphide and barite mineralization (between
13
14 82 ~5 and 40 meters thick). This provides an opportunity to address a number of questions relating
15
16 83 to seawater paleoredox during the Late Devonian and possible relationships with SHMS
17
18 84 mineralisation, including: (1) is there any evidence of a hydrothermal Mo flux at Macmillan Pass,
19
20 85 and if so, what is the isotopic composition? 2) How does the Selwyn Basin compare in terms of
21
22 86 paleoredox to other sedimentary basins hosting organic rich mudstones? 3) Is there a clear genetic
23
24 87 relationship between seawater paleoredox and sulphide mineralisation?
25
26
27
28
29
30

31 89 **METHODS**

32 90 *Samples*

33
34
35 91 Samples were collected from three correlated drill-holes (76-17, TYK-5 and TYK-1; Fig.
36
37 92 2C and 3), including 37 samples of un-mineralised mudstones and five samples from the
38
39 93 mineralised hydrothermal vent at the Tom deposit (Fig. 4). The stockwork veining in the vent
40
41 94 complex occurs immediately beneath the bedded mineralisation (see TYK-1 in Fig. 3 and Fig. 4),
42
43 95 and represents the main conduit of hydrothermal upflow in the SHMS systems at Macmillan Pass
44
45 96 (Magnall et al. 2016a).
46
47

48
49 97 Hand specimens of the un-mineralised mudstones were examined under a binocular
50
51 98 microscope to identify small-scale sedimentological features, and sub-samples were cut parallel
52
53 99 to bedding for geochemical analysis, minimising the vertical stratigraphic thickness of the sample
54
55 100 (< 2cm; Fig. 4). Care was taken to collect only the most homogenous, fine-grained samples, and
56
57 101 those containing high concentrations of euhedral pyrite, obvious detrital input (e.g. silt beds), and
58
59 102 any evidence of alteration (veining; hydrothermal or tectonic) were avoided. The vent complex
60
61
62
63
64
65

1
2
3
4 103 samples preserve an assemblage of ankerite veining and massive sulphide mineralisation within
5
6 104 variably altered organic-rich mudstone. The hydrothermal fluid entering the vent complex was
7
8 105 hot ($> 250\text{ }^{\circ}\text{C}$) and reducing ($f\text{O}_2 = 10^{-35}$) but rapidly cooled upon mixing with diagenetic fluids
9
10 106 (Magnall et al., 2016a).

11
12
13 107 *Chemical analyses*

14
15 108 Bulk rock powders for all samples (un-mineralised mudstones and mineralised vent
16
17 109 samples) were analysed for trace elements by aqua-regia digestion and ICP-MS at ACME
18
19 110 laboratories (Vancouver, Canada). Data quality and accuracy were monitored through the
20
21 111 analysis of in-house laboratory quartz blanks and internal standards, and the insertion of blind
22
23 112 quartz blanks and certified reference materials with the unknowns. As the un-mineralised
24
25 113 mudstones and mineralised vent complex samples have substantially different matrixes, different
26
27 114 reference materials were used; the SBC-1 and SGR-1b (USGS standards) were used for the
28
29 115 mudstones whereas OREAS standards (131a and 134a) were used for the mineralised vent
30
31 116 complex samples. The measured concentrations of the reference materials were always within the
32
33 117 certified range.

34
35
36
37 118 For the un-mineralised mudstones, the sequential extraction technique of Poulton and
38
39 119 Canfield (2005) was used to quantify highly reactive Fe (Fe_{HR}), which represents Fe incorporated
40
41 120 into pyrite (Fe_{PY}), carbonates (e.g. ankerite, siderite; Fe_{CARB}), ferric oxides (goethite, hematite;
42
43 121 Fe_{OX}), and magnetite (Fe_{MAG}). This involved the sequential extraction of Fe_{CARB} by a sodium
44
45 122 acetate leach (48 h at 50°C), Fe_{OX} by sodium dithionite leach (2 h at room temperature) and
46
47 123 Fe_{MAG} by ammonium oxalate leach (6 h at room temperature). Atomic absorption spectroscopy
48
49 124 (AAS) was then used to quantify the Fe in each sequential extraction. The Fe_{PY} fraction was
50
51 125 calculated from the extraction of sulphide as Ag_2S following a hot chromous chloride distillation
52
53 126 (Canfield et al., 1986). The relative standard deviation of repeat analyses of Fe_{PY} was 14% ($n =$
54
55 127 6), and for all other extractions $< 8\%$ ($n = 13$).

1
2
3
4 128 *Isotopic analyses*

5
6 129 Molybdenum isotope analyses were performed at the W.M. Keck Foundation Laboratory
7
8 130 for Environmental Biogeochemistry (Arizona State University) on a Thermo Finnigan Neptune
9
10 131 MC-ICP-MS with an Elemental Scientific Apex-Q and a PFA nebuliser. Splits of the same bulk
11
12 132 rock powders of un-mineralised mudstone were ashed at 550°C overnight to degrade organic
13
14 133 matter. Aliquots of 100 mg were sonicated in a combination of trace-metal-grade nitric and
15
16 134 hydrofluoric acids, then heated in sealed Teflon vessels at 120°C overnight. This was followed by
17
18 135 nitric and hydrochloric acids if digestion was not complete. Acids were evaporated off under
19
20 136 HEPA filtered air, and samples were re-dissolved in 6 M trace metal grade hydrochloric acid.
21
22 137 Samples were purified using a two-column method previously reported (Duan et al., 2010). In
23
24 138 brief, Biorad AG1X-8 anion resin is used to separate Fe and Mo from the resin; the matrix is
25
26 139 eluted in 6M HCl, and the Fe and Mo are co-eluted in 1 M HCl. Biorad AG50WX-8 cation
27
28 140 exchange resin is used to sequester Fe in 0.5 M HCl, and elute Mo. To correct for instrumental
29
30 141 mass bias and isobaric interferences, samples were doubled-spiked with a calibrated ⁹⁷Mo–¹⁰⁰Mo
31
32 142 spike. The following isotopes were measured for 4.1 seconds at 100 cycles per analysis: ⁹¹Zr,
33
34 143 ⁹²Mo, ⁹⁴Mo, ⁹⁵Mo, ⁹⁶Mo, ⁹⁷Mo, ⁹⁸Mo, ⁹⁹Ru and ¹⁰⁰Mo. All Mo isotopes were corrected for mass
35
36 144 bias and isobaric interferences with Zr (⁹²Zr, ⁹⁴Zr and ⁹⁶Zr).

37
38 145 Sample measurements were bracketed (every two analyses) by an in house standard,
39
40 146 RochMo2 (Johnson Matthey Chemical, Specpure ICP-MS standard, Stock #35758, Lot
41
42 147 #802309E). Every 10 samples four additional secondary standards were analysed, including NIST
43
44 148 SRM3134 (Goldberg et al. 2013), KyotoMo (In-house ICP standard, Kyoto University),
45
46 149 ImperialMo (in-house ICP standard, Imperial University) and SDO-1 (USGS rock reference
47
48 150 material). The Mo isotope data are presented as delta (δ) values as the parts per thousand (‰)
49
50 151 deviation in ⁹⁸Mo/⁹⁵Mo relative to the standard:

51
52
53
54
55
56
57
58 152
$$\delta^{98}\text{Mo} (\text{‰}) = \left\{ \left[\frac{(^{98}\text{Mo}/^{95}\text{Mo})_{\text{sample}}}{(^{98}\text{Mo}/^{95}\text{Mo})_{\text{standard}}} \right] - 1 \right\} \times 1000$$

59
60
61
62
63
64
65

1
2
3
4 153 The reproducibility of all analysed standard materials compare well with the long-term
5
6 154 values. The measured value for NIST SRM 3134 ($+0.31\text{‰} \pm 0.04$, 2σ ; $n = 12$) is slightly higher
7
8 155 than the value determined for this reference material ($+0.25\text{‰}$; Goldberg et al., 2013), and 0.06‰
9
10 156 has been subtracted from each sample so that data are reported relative to this interlaboratory
11
12 157 scale (Nägler et al., 2014).
13
14

15 158

17 159 **RESULTS**

19
20 160 The major element chemistry of the un-mineralised mudstones has already been
21
22 161 published in Magnall et al. (2015) and is supplemented in Table 1 by trace element data and 5
23
24 162 samples from the vent complex (this study). All chemical (Fe speciation) and Mo isotope data
25
26 163 are summarised in Table 2, together with bulk rock $\delta^{34}\text{S}$ values reported by Magnall et al. (2016b)
27
28 164 that were produced on the same un-mineralised mudstone samples. Down-hole plots of Fe
29
30 165 speciation parameters ($\text{Fe}_{\text{HR}}/\text{Fe}_{\text{T}}$, $\text{Fe}_{\text{PY}}/\text{Fe}_{\text{HR}}$) and Mo geochemistry ($\delta^{98}\text{Mo}$, ppm) are presented
31
32 166 in Figure 5. Where median values are given in the following text, the interquartile range (Q1 to
33
34 167 Q3) is included in parentheses. The un-mineralised mudstones contain high levels of SiO_2
35
36 168 (median $77.0\text{ wt.}\%$; Q1 to Q3 = 72.9 to 80.6). The SiO_2 is largely of biogenic origin (see Magnall
37
38 169 et al. 2015), however total Fe (Fe_{T}) has not been diluted below the concentration considered to
39
40 170 give reliable Fe paleo-redox data ($\text{Fe}_{\text{T}} = 0.5\text{ wt.}\%$; Clarkson et al., 2014); samples from drill-hole
41
42 171 (DH) 76-17 contain median Fe_{T} of $1.47\text{ wt.}\%$ (Q1 to Q3 = 1.19 to 1.83) and DH-TKY-5 of 2.41
43
44 172 $\text{wt.}\%$ (Q1 to Q3 = 1.32 to 2.90). Samples from DH-76-17 and DH-TYK-5 preserve contrasting
45
46 173 $\text{Fe}_{\text{T}}/\text{Al}$ ratios, with respective median values of 0.38 (Q1 to Q3 = 0.31 to 0.45) and 0.61 (Q1 to
47
48 174 Q3 = 0.29 to 0.67). In samples from DH-TYK-5, $\text{Fe}_{\text{T}}/\text{Al}$ forms a positive correlation ($R^2 = 0.72$)
49
50 175 with bulk rock $\delta^{34}\text{S}$ values (Fig. 6).
51
52

53
54 176 In terms of Fe speciation, highly reactive iron (Fe_{HR}), which is a summation of Fe in
55
56 177 pyrite (Fe_{PY}), carbonate (Fe_{CARB}), oxide phases (Fe_{OX}) and magnetite (Fe_{MAG}), comprises a
57
58 178 major proportion of total Fe (Fe_{T}) in both drill-holes (Fig. 5). Median $\text{Fe}_{\text{HR}}/\text{Fe}_{\text{T}}$ values are 0.86
59
60
61
62
63
64
65

1
2
3
4 179 (Q1 to Q3 = 0.81 to 0.94) and 0.98 (Q1 to Q3 = 0.95 to 1.02) for samples from 76-17 and TYK-5,
5
6 180 respectively. The fraction of Fe_{HR} present as Fe_{PY} is high in both drill-holes (Fig. 5), with median
7
8 181 values for Fe_{PY}/Fe_{HR} of 0.72 (Q1 to Q3 = 0.65 to 0.76) in samples from DH-76-17 and 0.85 (Q1
9
10 182 to Q3 = 0.78 to 0.86) for samples from TYK-5. Most of the un-sulphidised Fe_{HR} occurs as
11
12 183 Fe_{CARB}, with minor amounts of Fe_{OX} and Fe_{MAG} (see Table 1).
13
14

15 184 In terms of trace metals (see Fig. 7), the 5 mineralised samples contain high but variable
16
17 185 levels of Zn (0.8 wt.%, < 0.1 to 2.5) and Pb (3.8 wt.%, 0.1 to 8.2), but low levels of Mo (3 to 5
18
19 186 ppm). In contrast, the un-mineralised mudstones contain < 100 ppm Pb and mostly < 1000 ppm
20
21 187 Zn. Compared to the mineralised vent samples, however, Mo is enriched in the mudstones (18
22
23 188 ppm, Q1 to Q3 = 14 to 21). The mudstone samples have a narrow, normally distributed range of
24
25 189 $\delta^{98}\text{Mo}$ values (0.48‰ \pm 0.11), with no systematic relationship between $\delta^{98}\text{Mo}$ values and
26
27 190 Fe_{PY}/Fe_{HR} (Fig. 5). There are weak correlations between Mo and TOC ($r^2 = 0.37$; Fig. 8) and
28
29 191 between Mo and TOC/P ($r^2 = 0.43$; Fig. 9a), and a stronger correlation between TOC/P and P/Al
30
31 192 ($r^2 = 0.59$; Fig. 9b). Also included in Figures 8 and 9 are recently published data for correlative
32
33 193 mudstones from the Richardson Trough (Fraser and Hutchison, 2017), which is a northerly
34
35 194 extension of the Selwyn Basin (Figure 1).
36
37
38
39
40
41
42
43
44
45
46
47
48
49
50
51
52
53
54
55
56
57
58
59
60
61
62
63
64
65

1
2
3
4 **195 DISCUSSION**

5
6 **196 *Iron Geochemistry***

7
8 **197** The total Fe (Fe_T) budget of marine sediments is comprised of Fe_{HR} , which represents Fe
9
10 **198** that may undergo redox-controlled mineralogical transformations during diagenesis, together with
11
12 **199** poorly reactive and unreactive silicate Fe (Raiswell and Canfield, 1998). When normalised to Al
13
14 **200** (which in most sedimentary environments is immobile), changes in Fe_T/Al typically reflect redox-
15
16 **201** controlled changes in the Fe_{HR} budget of sediments (Lyons and Severmann, 2006; Scholz et al.,
17
18 **202** 2014). For example, when dissolution of insoluble Fe (oxy)hydroxides occurs in euxinic basins,
19
20 **203** water column (syngenetic) pyrite formation can result in underlying sediments developing high
21
22 **204** Fe/Al ratios relative to lithogenic background (Lyons and Severmann, 2006). In contrast, in parts
23
24 **205** of the modern ocean where both low oxygen and low sulphide concentrations occur, Fe
25
26 **206** (oxy)hydroxide dissolution in sediment pore fluids results in the release of Fe^{2+} to the water
27
28 **207** column and the development of relatively low sedimentary Fe/Al ratios (Scholz et al., 2014).
29
30

31
32 **208** The median Fe/Al value for samples from DH-76-17 (0.38; Fig. 6a) overlaps with
33
34 **209** correlative mudstones from the Richardson Trough (Fraser and Hutchison, 2017). Combined, the
35
36 **210** Fe/Al value of samples from the Richardson Trough and DH-76-17 may indicate a regional
37
38 **211** lithogenic background (e.g. Scholz et al., 2014) that is lower than the upper continental crust
39
40 **212** value that is commonly used as a reference for shale (0.44; McLennan, 2001). In contrast, the
41
42 **213** Fe/Al in samples from DH-TYK-5 is higher (median = 0.61), which could indicate Fe_{HR}
43
44 **214** enrichment associated with syngenetic pyrite formation in a euxinic water column (Lyons and
45
46 **215** Severmann, 2006). Indeed, there is a good correlation between increasing Fe/Al (Fig. 6b), and
47
48 **216** more positive bulk rock $\delta^{34}S$ values that are typical of pyrite formation in sulphate limited
49
50 **217** conditions (Gomes and Hurtgen, 2015). Sulphate limited conditions, however, can occur on
51
52 **218** different scales; for example, within the water column at a basin scale (Newton et al., 2011) or at
53
54 **219** a more local scale within diagenetic pore fluids (Borowski et al., 2013). Indeed, recent in situ
55
56 **220** isotopic analyses of pyrite at Macmillan Pass has established that positive $\delta^{34}S$ values ($> 15\text{‰}$)
57
58
59
60
61
62
63
64
65

1
2
3
4 221 developed during diagenesis (i.e. at a local scale), close to the sulphate methane transition zone
5
6 222 (SMTZ) (Magnall et al., 2016b). Thus, the trend towards more positive bulk rock $\delta^{34}\text{S}$ values at
7
8 223 higher Fe/Al in samples from DH-TYK-5 (Fig. 6b) is evidence that Fe enrichment corresponds
9
10 224 with a greater proportion of pyrite formed at the SMTZ relative to pyrite formed via bacterial
11
12 225 sulphate reduction (BSR). This interpretation is similar to recent work that has documented
13
14 226 increasing $\text{Fe}_{\text{PY}}/\text{Fe}_{\text{HR}}$ and $\delta^{34}\text{S}$ values at the SMTZ along the continental margin of the South
15
16 227 China Sea (Lin et al., 2016). In contrast, there is no correlation between Fe/Al and $\delta^{34}\text{S}$ in
17
18 228 samples from DH-76-17, indicating the predominant generation of pyrite formed during early
19
20 229 diagenesis via BSR and there was minimal subsequent Fe enrichment. Nevertheless, in both drill
21
22 230 holes (TYK-5 and 76-17) Fe_{HR} still represents the predominant component of Fe_{T} and greatly
23
24 231 exceeds the threshold for deposition under anoxic conditions ($\text{Fe}_{\text{HR}}/\text{Fe}_{\text{T}} > 0.38$; Poulton and
25
26 232 Raiswell, 2002; Raiswell and Canfield, 1998).

27
28
29
30
31 233 The degree to which Fe_{HR} is converted to Fe_{PY} can be used to distinguish between anoxic
32
33 234 non-sulphidic (ferruginous) and anoxic sulphidic (euxinic) conditions (Poulton and Canfield,
34
35 235 2005). High levels of pyritisation ($\text{Fe}_{\text{PY}}/\text{Fe}_{\text{HR}} > 0.7$) suggest a persistently euxinic water-column,
36
37 236 whereas lower values ($\text{Fe}_{\text{PY}}/\text{Fe}_{\text{HR}} < 0.7$) are more consistent with varying degrees of pyritisation
38
39 237 within sulphidic pore fluids (i.e. beneath anoxic, non-sulphidic waters, which are commonly
40
41 238 ferruginous) or under weakly or intermittently euxinic conditions (Poulton and Canfield, 2011).
42
43 239 Applying this framework to samples from Macmillan Pass is only appropriate for samples from
44
45 240 DH-76-17, considering the evidence for diagenetic pyrite enrichment (Fig. 6b). For these
46
47 241 samples, a median value for $\text{Fe}_{\text{PY}}/\text{Fe}_{\text{HR}}$ of 0.72 represents a high level of pyritisation that does
48
49 242 not strongly distinguish between euxinic or ferruginous conditions. Indeed, ferruginous settings
50
51 243 that are prone to intermittent euxinia result in similar levels of pyritisation (e.g. Poulton et al.,
52
53 244 2015). As such, it is necessary to evaluate additional redox proxies to ensure an accurate
54
55 245 interpretation of seawater paleoredox at Macmillan Pass.
56
57
58
59
60
61
62
63
64
65

1
2
3
4 246

5
6 247 *Molybdenum Geochemistry*

7
8 248 In oxic seawater, molybdenum is present as the conservative molybdate anion (MoO_4^{2-}),
9
10 249 which adsorbs onto ferromanganese oxides resulting in a large isotopic fractionation ($\Delta^{98}\text{Mo}_{\text{SW-OX}}$
11
12 250 $= \delta^{98}\text{Mo}_{\text{SW}} - \delta^{98}\text{Mo}_{\text{OX}} \leq 3\text{‰}$; Barling et al., 2001; Siebert et al., 2003; Barling and Anbar, 2004;
13
14 251 Poulson et al., 2006). In contrast, when sulphide concentrations exceed 11 μM (Erickson and
15
16 252 Helz, 2000), the complete transformation of molybdate to reactive thiomolybdate species
17
18 253 (substitution of oxygen by sulphur; $\text{MoO}_x\text{S}_{4-x}^{2-}$) may result in minimal fractionation of $\delta^{98}\text{Mo}$
19
20 254 values between sediment and seawater or pore fluid (e.g. Nögler et al., 2005; Neubert et al.,
21
22 255 2008). This can also result in high sedimentary Mo enrichments (> 100 ppm) in unrestricted
23
24 256 euxinic basins (Scott and Lyons, 2012).

25
26
27
28
29 257 There are currently two studies that provide constraints for the $\delta^{98}\text{Mo}$ value of Late
30
31 258 Devonian seawater (Gordon et al., 2009; Dahl et al. 2010), albeit from two different periods (Fig.
32
33 259 10). Both studies present data generated from analyses of organic-rich mudstones, where
34
35 260 deposition in a euxinic basin is inferred from high levels of pyritisation. The $\delta^{98}\text{Mo}$ values
36
37 261 reported in either study ($\sim 1.5 - 2.0\text{‰}$) are lower than modern seawater (2.4‰), which provides
38
39 262 evidence that the global oceans during the Late Devonian may have been less oxygenated,
40
41 263 although it is difficult to accurately constrain the size of the ferruginous vs. euxinic sinks (Gordon
42
43 264 et al., 2009; Dahl et al. 2010).

44
45
46
47 265 At Macmillan Pass, the narrow distribution of $\delta^{98}\text{Mo}$ values ($+0.48\text{‰} \pm 0.20$) is between
48
49 266 0.7‰ and 1.0‰ lower than current constraints for Late Devonian seawater ($\delta^{98}\text{Mo} = +1.4\text{‰}$ to
50
51 267 $+1.6\text{‰}$; Gordon et al., 2009). Considering the equivocal constraints provided by the Fe based
52
53 268 paleoredox proxies, there are three possible explanations for the $\delta^{98}\text{Mo}$ values: (1) the Mo has a
54
55 269 predominantly hydrothermal rather than authigenic origin; (2) Mo was fractionated from seawater
56
57
58
59
60
61
62
63
64
65

1
2
3
4 270 in a non-euxinic setting; (3) deposition occurred in a euxinic setting, with a $\delta^{98}\text{Mo}$ value of
5
6 271 Frasnian seawater that was lower than the constraints for Givetian and Fammenian seawater.

7
8 272 Starting with option (1), the $\delta^{98}\text{Mo}$ values at Macmillan Pass (Fig. 10) overlap with
9
10 273 analyses of modern low-temperature hydrothermal fluids that circulate through sediment covered
11
12 274 ridge axis systems ($\delta^{98}\text{Mo} = 0.8\text{‰}$; McManus et al., 2002). In these modern settings, the Mo is
13
14 275 thought to be derived from fluid-rock interaction with basalt (\pm some diagenetic Mo component;
15
16 276 Wheat et al., 2002). The majority of studies on Mo solubility in hydrothermal fluids focus on
17
18 277 magmatic hydrothermal systems, where Mo is shown to partition into the vapour phase (Rempel
19
20 278 et al., 2009). The hydrothermal systems at Macmillan Pass preserve no evidence of direct
21
22 279 magmatic input (Magnall et al., 2016a), and in the hot ($> 250^\circ\text{C}$), reducing ($f\text{O}_2 = 10^{-35}$) single
23
24 280 phase fluids, Mo^{4+} rather than the more soluble Mo^{6+} will have been stable. The vent fluids are
25
26 281 therefore unlikely to have produced a major hydrothermal flux of Mo, which is supported by the
27
28 282 negative correlation between Mo and Pb+Zn concentrations in samples from the mineralised vent
29
30 283 complex and organic-rich mudstones (Fig. 7). Having established that the Mo in the Macmillan
31
32 284 Pass mudstones is predominantly authigenic (rather than hydrothermal), the mechanism of Mo
33
34 285 enrichment (option 2) and whether this can provide any information on Late Devonian seawater
35
36 286 (option 3) will now be considered.

37
38 287 Organic-rich mudstones commonly preserve a strong relationship between Mo and TOC
39
40 288 (Algeo et al. 2007). In modern, strongly restricted, anoxic basins, the efficient transfer of Mo
41
42 289 from seawater to sediment results in Mo depletion over time, such that sediments are
43
44 290 characterised by low Mo/TOC ratios (e.g. Black Sea; Algeo and Lyons, 2006). Where there is
45
46 291 strong co-variation between Mo and TOC, it is also possible to place more quantitative
47
48 292 constraints on both the size of the Mo reservoir and also deep-water residence times of Mo within
49
50 293 a basin (Algeo et al., 2007). For the Macmillan Pass mudstones, Mo and TOC are only weakly
51
52 294 correlated ($r^2 = 0.37$; Fig. 8), with a narrow range in Mo/TOC (3.5 to 8 ppm/wt.%) that overlaps
53
54
55
56
57
58
59
60
61
62
63
64
65

1
2
3
4 295 with Black Sea sediments. Similar Mo/TOC values are also preserved in the Richardson Trough
5
6 296 samples (Fraser and Hutchison, 2017), although for these samples there is no correlation between
7
8 297 Mo and TOC ($r^2 = 0.02$).
9

10 298 The contrasting redox chemistries of Mo and U can lead to the development of
11
12
13 299 characteristic trends that provide information on both the redox and hydrography of depositional
14
15 300 environments (Algeo and Tribovillard, 2009). For example, reduction of soluble U^{6+} to insoluble
16
17 301 U^{4+} occurs at a similar redox potential to the Fe^{3+} – Fe^{2+} transition, meaning that U enrichment
18
19 302 occurs under less reducing conditions than for Mo, which requires sulphidic conditions (Morford
20
21 303 et al., 2009). This means that as conditions become more reducing (i.e. suboxic – anoxic –
22
23 304 euxinic), there is a progressive enrichment of Mo relative to U in open marine settings (Algeo and
24
25 305 Tribovillard, 2009). In contrast, in basins that are both reducing and have longer deep-water
26
27 306 renewal times (i.e. basin restriction), water mass chemistry can evolve to lower Mo/U ratios (e.g.
28
29 307 Black Sea; Algeo and Tribovillard, 2009). In Figure 11, Mo and U enrichment factors (EFs) have
30
31 308 been calculated for samples from Macmillan Pass, and compared to correlative Late Devonian
32
33 309 mudstones from the Richardson Trough (Fraser and Hutchison, 2017). The two Selwyn Basin
34
35 310 data sets form a linear trend at a Mo/U ratio higher than seawater. This trend is thought to result
36
37 311 from the complexation of Mo to Fe and Mn (oxyhydr)oxides (particulate shuttle; Algeo and
38
39 312 Tribovillard, 2009), which occurs at the chemocline between oxic and anoxic water masses
40
41 313 (Berrang and Grill, 1974; Dellwig et al., 2010). More recently it has been demonstrated that
42
43 314 nitrate, not oxygen, can act as the terminal electron acceptor in modern oxygen minimum zones
44
45 315 (Scholz et al. 2016); in these settings, Fe^{2+} released from sediment pore fluids is oxidized at the
46
47 316 chemocline between weakly sulphidic and nitrogenous conditions in near bottom waters.
48
49 317 Importantly, the location of this chemocline exerts a control on the degree of trace element
50
51 318 enrichment (Algeo and Tribovillard, 2009). For example, in stratified basins (e.g. the Black Sea)
52
53 319 where the chemocline is located high in the water column, particulates undergo reductive
54
55 320 dissolution and Mo is released before reaching the sediment (Crusius et al., 1996). In contrast,
56
57
58
59
60
61
62
63
64
65

1
2
3
4 321 Mo transfer can be enhanced when there is redox variability on short timescales, particularly
5
6 322 when the chemocline is located close to the sediment-water interface (SWI). The suppression of
7
8 323 Mo_{EF} values at higher U_{EF} (i.e. a flattening of the Mo-U co-variation), which is a trend typically
9
10 324 encountered in strongly restricted basins, is not preserved in the Macmillan Pass samples (Fig.
11
12 325 11). It is worth highlighting that current paleogeographic reconstructions show the Selwyn Basin
13
14 326 was no less connected to the global ocean than other Late Devonian basins on the Laurentian
15
16 327 margin (Fig. 1). Furthermore, the Mo-U co-variation is similar to trends observed both in
17
18 328 moderately restricted basins such as the Cariaco Basin (Venezuela; Algeo and Tribovillard, 2009)
19
20 329 and the Baltic Sea (Scholz et al., 2013), as well as upwelling zones in open ocean settings (e.g.
21
22 330 Peru; Scholz et al., 2011). This appears to contrast with the low Mo/TOC ratios at Macmillan
23
24 331 Pass and Richardson Trough. However, the stronger co-variation between Mo and U
25
26 332 demonstrates the predominant mechanism of Mo enrichment occurred via the particulate shuttle,
27
28 333 weakening any relationship between Mo and TOC. As such, it may be difficult to make a reliable
29
30 334 interpretation of deep-water renewal times when a relationship between Mo and TOC cannot be
31
32 335 established.

336 337 *The particulate shuttle and Mo isotope fractionation*

338 The identification of a particulate shuttle trend provides valuable context for the
339 interpretation of $\delta^{98}Mo$ values at Macmillan Pass, which are offset from available constraints for
340 Late Devonian seawater (+1.5 to +2.0‰; Dahl et al., 2010; Gordon et al., 2009). Although Mo
341 isotopes cannot directly help to address the issue of basin restriction, similar isotopic
342 fractionations are preserved in modern anoxic, open-ocean settings (McManus et al., 2002;
343 Poulson et al., 2006; Dickson et al., 2014).

344 Using the constraints for Late Devonian seawater, the $\delta^{98}Mo$ values of the Macmillan
345 Pass mudstones (+0.7 to +1.0‰) correspond with the isotopic fractionation that occurs during Mo

1
2
3
4 346 adsorption to Fe (oxyhydr)oxides (Goldberg et al., 2009). In samples without major diagenetic
5
6 347 pyrite enrichment ($Fe/Al < 0.44$) there is a positive correlation between Fe/Al and $\delta^{98}Mo$ values
7
8 348 (Fig. 12a), providing evidence that the redox geochemistry of Fe and Mo may have been linked.
9
10 349 A major finding of Goldberg et al. (2009) was that the mineralogy of Fe (oxyhydr)oxides exerts a
11
12 350 control on $\delta^{98}Mo$ values, as complexation with magnetite, goethite and ferrihydrite produces
13
14 351 respective fractionations ($\Delta^{98}Mo$) of $0.83\% \pm 0.60$, $1.11\% \pm 0.15$ and $1.40\% \pm 0.48$. Assuming
15
16 352 that $\delta^{98}Mo$ values are controlled predominantly by Fe (oxyhydr)oxide mineralogy, the correlation
17
18 353 between Fe/Al and $\delta^{98}Mo$ values may indicate that a change in mineralogy was accompanied by
19
20 354 an increase in delivery of Fe_{HR} .
21
22
23
24

25 355 As sedimentary Mo enrichment appears to be controlled primarily via the particulate
26
27 356 shuttle, the correlation between Fe/Al and $\delta^{98}Mo$ values could also be explained by a simple
28
29 357 closed system Rayleigh fractionation model (Fig. 12b). In terms of the boundary conditions, the
30
31 358 model starts with a $\delta^{98}Mo$ value of 1.5% , taken as a lower limit for Late Devonian seawater
32
33 359 (Dahl et al., 2010; Gordon et al., 2009). A major assumption of this model is that the $\delta^{98}Mo$ value
34
35 360 of seawater remained constant throughout the stratigraphic interval, which could represent
36
37 361 deposition over more than 7 Myr (Fig. 10). From this starting point ($\delta^{98}Mo = 1.5\%$), a
38
39 362 fractionation factor intermediate between ferrihydrite ($\alpha = 0.99989$) and goethite ($\alpha = 0.99986$) is
40
41 363 used, which corresponds with the lowermost $\delta^{98}Mo$ values at Macmillan Pass (0.33%). The
42
43 364 model then produces the narrow distribution of $\delta^{98}Mo$ values without extensive depletion of Mo
44
45 365 in the residual fluid (see Fig. 12b). In this case, the residual fluid is unlikely to represent global
46
47 366 seawater, the $\delta^{98}Mo$ value of which represents isotopic mass balance between all other Mo sinks.
48
49 367 Indeed, the good correlation between Fe/Al and $\delta^{98}Mo$ is evidence that a single, more localised
50
51 368 parameter (i.e. particulate shuttle) is responsible for the isotopic composition of Mo retained in
52
53 369 the sediment. Thus, the model demonstrates how the size of the Mo flux associated with the
54
55
56
57
58
59
60
61
62
63
64
65

1
2
3
4 370 particulate shuttle could produce small corresponding changes in the $\delta^{98}\text{Mo}$ value of soluble Mo
5
6 371 at the chemocline.
7
8
9 372

10 373 *Phosphorus cycling and productivity in the Selwyn Basin during the Late Devonian*
11
12
13

14 374 The anoxic, predominantly non-sulphidic conditions that prevailed at Macmillan Pass
15
16 375 during the Late Devonian will have played a key role in the cycling of phosphorus (e.g. März et
17
18 376 al., 2008), the availability of which controls primary productivity (Tyrrell, 1999). Unlike Fe, only
19
20 377 a minor fraction of the total phosphorus (P_T) in marine sediments is of detrital origin, and a major
21
22 378 component of P_T is associated with organic matter and Fe (oxyhydr)oxides (Algeo and Ingall,
23
24 379 2007). Depositional redox conditions, therefore, exert a strong control on the degree to which P is
25
26 380 retained within marine sediments, and as conditions become more reducing the regeneration of P
27
28 381 from organic matter and Fe (oxyhydr)oxides to seawater is enhanced (Ingall et al., 1993; Ingall
29
30 382 and Cappellen, 1990).
31
32
33

34 383 The TOC/P ratios of the Macmillan Pass samples are depleted relative to the Redfield
35
36 384 ratio (~106:1), which defines the TOC:P ratio of marine phytoplankton (Redfield, 1958). Low
37
38 385 TOC/P ratios often develop in sediments deposited under suboxic conditions, when there is
39
40 386 limited P regeneration back to the water column (e.g. Peruvian margin; Böning et al., 2004).
41
42 387 Moreover, the weak correlation between TOC/P and Mo_{EF} at Macmillan Pass is consistent with
43
44 388 the contrasting redox behaviours of P and Mo, with the latter being more sensitive to reduced
45
46 389 sulphur availability. Expanding this framework to samples from the Richardson Trough further
47
48 390 supports this model; here, high TOC/P values are coupled with more extreme Mo enrichments,
49
50 391 indicating extensive P recycling under more reducing (likely sulphidic) conditions.
51
52
53

54 392 At Macmillan Pass, the high levels of pyritisation, low TOC/P and intermediate Mo
55
56 393 enrichments are similar to those preserved in mudstones deposited in the proto North Atlantic
57
58 394 during the Cretaceous under ferruginous conditions (März et al., 2008). Nevertheless, considering
59
60
61
62
63
64
65

1
2
3
4 395 the high levels of pyritisation (≥ 0.7) in some Macmillan Pass samples, intermittent periods of
5
6 396 euxinia remain a possibility. Notably, continuous high resolution sampling of short stratigraphic
7
8 397 intervals has revealed a cyclicity in the development of ferruginous and euxinic conditions during
9
10 398 periods of major carbon burial (e.g. März et al., 2008; Poulton et al., 2015). Such redox cyclicity
11
12 399 likely has a key role in maintaining a balance between burial and regeneration of P, which
13
14 400 ultimately governs P availability, primary productivity and carbon burial over geologic timescales
15
16 401 (Van Cappellen and Ingall, 1994). Both at Macmillan Pass and Richardson Trough, the organic
17
18 402 rich mudstones are enriched in biogenic silica (>75 wt. %; Magnall et al. 2015, Fraser and
19
20 403 Hutchison, 2017), which provides evidence of high productivity during the Late Devonian. The
21
22 404 development of anoxic conditions, which were predominantly ferruginous but had potential for
23
24 405 intermittent euxinia, would therefore have had an important role in maintaining nutrient
25
26 406 availability and productivity on a regional scale.
27
28
29
30

31 407

32
33 408 *The role of seawater paleoredox in the formation of SHMS deposits*
34
35

36 409 Some of the early work on seawater paleoredox in the Selwyn Basin emphasised a link
37
38 410 between basin restriction, protracted water-column euxinia and sulphide formation (Goodfellow
39
40 411 et al., 1993; Turner, 1992). In this euxinic basin model, sulphide formation occurred within the
41
42 412 water column following exhalation of hydrothermal fluids above the SWI. However, the Fe
43
44 413 speciation and Mo isotope data presented for Macmillan Pass in this study provide no evidence of
45
46 414 sustained euxinia. Rather, sulphide was likely restricted to sediment pore fluids with an overlying
47
48 415 water column that was predominantly ferruginous.
49
50

51 416 In ferruginous settings, pyrite formation may be limited by the availability of sulphate
52
53 417 rather than organic carbon (Poulton and Canfield, 2011), an observation supported by recent work
54
55 418 proposing low concentrations of sulphate in Late Devonian seawater (Sim et al., 2015). Indeed,
56
57 419 low seawater sulphate may have been characteristic of much of the Early Paleozoic (Horita et al.,
58
59
60
61
62
63
64
65

1
2
3
4 420 2002). Two factors are important in this context: (1) under reducing conditions, sulphide
5
6 421 concentration imposes a limit on the solubility of base metals, and long periods of low seawater
7
8 422 sulphate may have facilitated the development of sulphide-poor, Pb-Zn-Fe enriched basinal fluids
9
10 423 (Wilkinson, 2014), and; (2) the formation of massive sulphide deposits close to the seafloor in a
11
12 424 non-euxinic setting requires the optimisation of other processes that concentrate reduced sulphur,
13
14 425 derived from seawater sulphate, into the host rock. Various pathways of sulphur enrichment have
15
16 426 been documented in the host rocks to SHMS mineralisation, including diagenetic barite formation
17
18 427 (Johnson et al., 2004), diagenetic sulphate reduction (e.g. Fallick et al., 2001; Magnall et al.,
19
20 428 2016b), and thermochemical sulphate reduction (Gadd et al., 2016; Magnall et al., 2016a). All
21
22 429 pathways are linked by organic carbon, and a common feature of emerging models for SHMS
23
24 430 mineralisation is their formation in continental margin environments with high levels of
25
26 431 biological productivity (e.g. Magnall et al., 2015; Reynolds et al., 2015; Slack et al., 2016).

30
31 432 Where SHMS deposits form via sub-seafloor replacement, there is clear potential for an
32
33 433 overlap between hydrothermal and diagenetic processes. Despite there being no direct modern
34
35 434 analogues for SHMS systems, hydrothermal activity in the Guaymas Basin serves as a useful
36
37 435 comparison, where rift-related hydrothermal activity is accompanied by the release of methane
38
39 436 within recently deposited sediments (Berndt et al., 2016). At Macmillan Pass, SHMS
40
41 437 mineralisation occurs where faults provide a flow path for metal-rich hydrothermal fluids (e.g.
42
43 438 Magnall et al., 2016a) to reach the shallow sub-surface environment. It is likely, therefore, that
44
45 439 the onset and development of hydrothermal activity at Macmillan Pass during the Late Devonian
46
47 440 would have resulted in the enhanced circulation of diagenetic fluids in sediments proximal to the
48
49 441 hydrothermal system. Clearly, in more dynamic diagenetic environments it is necessary to
50
51 442 evaluate multiple proxies when attempting to reconstruct seawater paleoredox. In coupling the Fe
52
53 443 and Mo based proxies in samples from a proximal and distal setting (with respect to SHMS
54
55 444 mineralisation), we have demonstrated how this approach can be made.
56
57
58
59
60
61
62
63
64
65

1
2
3
4 445 *CONCLUSIONS*

5
6 446 The co-variation between Mo and U in the combined data-sets from Macmillan Pass and
7
8 447 the Richardson Trough provides good evidence that the dominant mechanism of Mo enrichment
9
10 448 occurred via a particulate shuttle involving Fe (oxyhydr)oxides. This is further supported by the
11
12 449 $\delta^{98}\text{Mo}$ values preserved in mudstones at Macmillan Pass, which are fractionated from Late
13
14 450 Devonian seawater by 0.7 to 1.0 ‰. The incomplete pyritisation of Fe_{HR} ($\leq 70\%$) in samples from
15
16 451 DH-76-17 provides evidence that conditions were predominantly ferruginous, with potential for
17
18 452 intermittent euxinia. At Macmillan Pass, anoxic, non-sulphidic conditions led to P enrichment
19
20 453 and TOC/P ratios below the Redfield ratio (~106:1). This contrasts with the high TOC/P ratios in
21
22 454 the Richardson Trough, which are combined with much greater Mo enrichments. Here,
23
24 455 regeneration of P within the water column combined with high levels of Mo provides convincing
25
26 456 evidence of more persistent water column euxinia. Nevertheless, the dominant mechanism of Mo
27
28 457 enrichment was still via the particulate shuttle, and high but uniform Mo/U values provide no
29
30 458 evidence of long deep-water renewal times and strong basin restriction. At Macmillan Pass,
31
32 459 formation of SHMS deposits in non-euxinic environments therefore requires the optimisation of
33
34 460 other factors (e.g. diagenetic sulphate reduction, barite replacement) that contribute to the sulphur
35
36 461 budget of the host rock. At a first order, these factors are controlled by high primary productivity
37
38 462 and enhanced carbon burial, which therefore represent the most important variables in the
39
40 463 development of effective chemical traps for high-grade SHMS deposits.
41
42
43
44
45
46
47
48

49 465 **ACKNOWLEDGEMENTS**

50
51 466 The first author would like to thank Romain Guilbaud for his assistance with the Fe
52
53 467 speciation experiments. Funding acknowledgement is given to a Helmholtz-Rekrutierungsinitiative,
54
55 468 and NSERC Discovery Grant to S. Gleeson and the TGI4 initiative (Geological Survey of
56
57 469 Canada). Reviews by Thomas Algeo, Nicolas Tribouillard, Fernando Tornos and in particular the
58
59
60
61
62
63
64
65

1
2
3
4
5
6
7
8
9
10
11
12
13
14
15
16
17
18
19
20
21
22
23
24
25
26
27
28
29
30
31
32
33
34
35
36
37
38
39
40
41
42
43
44
45
46
47
48
49
50
51
52
53
54
55
56
57
58
59
60
61
62
63
64
65

470 comments of an anonymous reviewer are graciously acknowledged for helping improve the
471 manuscript.

1
2
3
4 472 **REFERENCES**

- 5
6 473 Abbott, J.G., Turner, R.J., 1991. Character and paleotectonic setting of Devonian stratiform
7
8 474 sediment-hosted Zn, Pb, Ba deposits, Macmillan Fold Belt, Yukon, in: Abbott, J.G., Turner,
9
10 475 R.J. (Eds.), Geological Survey of Canada Open File 2169. pp. 99–136.
11
12
13 476 Algeo, T.J., Lyons, T.W., 2006. Mo–total organic carbon covariation in modern anoxic marine
14
15 477 environments: Implications for analysis of paleoredox and paleohydrographic conditions.
16
17 478 *Paleoceanography* 21, 1–23.
18
19 479 Algeo, T.J., Ingall, E., 2007. Sedimentary Corg:P ratios, paleocean ventilation, and Phanerozoic
20
21 480 atmospheric pO₂. *Palaeogeog. Palaeoclim. Palaeoeco.* 256, 130–155.
22
23
24 481 Algeo, T.J., Lyons, T.W., Blakey, R.C., Over, J.D., 2007. Hydrographic conditions of the
25
26 482 Devono–Carboniferous North American Seaway inferred from sedimentary Mo–TOC
27
28 483 relationships. *Palaeogeog. Palaeoclim. Palaeoeco.* 256, 204–230.
29
30
31 484 Algeo, T.J., Tribovillard, N., 2009. Environmental analysis of paleoceanographic systems based
32
33 485 on molybdenum–uranium covariation. *Chem. Geol.* 268, 211–225.
34
35 486 Arnold, G.L., Anbar, A.D., Barling, J., Lyons, T.W., 2004. Molybdenum Isotope Evidence for
36
37 487 Widespread Anoxia in Mid-Proterozoic Oceans. *Science* 304, 87–90.
38
39 488 Barling, J., Anbar, A.D., 2004. Molybdenum isotope fractionation during adsorption by
40
41 489 manganese oxides. *Earth Planet. Sci. Lett.* 217, 315–329.
42
43 490 Barling, J., Arnold, G.L., Anbar, A.D., 2001. Natural mass-dependent variations in the isotopic
44
45 491 composition of molybdenum. *Earth Planet. Sci. Lett.* 193, 447–457.
46
47
48 492 Berndt, C., Hensen, C., Mortera-Gutierrez, C., Sarkar, S., Geilert, S., Schmidt, M., Liebetrau, V.,
49
50 493 Kipfer, R., Scholz, F., Doll, M., Muff, S., Karstens, J., Planke, S., Petersen, S., Böttner, C.,
51
52 494 Chi, W.C., Moser, M., Behrendt, R., Fiskal, A., Lever, M.A., Su, C.C., Deng, L.,
53
54 495 Brennwald, M.S., Lizarralde, D., 2016. Rifting under steam - how rift magmatism triggers
55
56 496 methane venting from sedimentary basins. *Geology* 44, 767–770.
57
58
59 497 Berrang, P.G., Grill, E. V., 1974. The effect of manganese oxide scavenging on molybdenum in
60
61
62
63
64
65

1
2
3
4
5
6
7
8
9
10
11
12
13
14
15
16
17
18
19
20
21
22
23
24
25
26
27
28
29
30
31
32
33
34
35
36
37
38
39
40
41
42
43
44
45
46
47
48
49
50
51
52
53
54
55
56
57
58
59
60
61
62
63
64
65

498 saanich inlet, British Columbia. *Mar. Chem.* 2, 125–148.

499 Blakey, R., 2013. Late Devonian from Map Series. North American Key Time Slices © 2013
500 Colorado Plateau Geosystems Inc.

501 Böning, P., Brumsack, H.-J., Böttcher, M.E., Schnetger, B., Kriete, C., Kallmeyer, J., Borchers,
502 S.L., 2004. Geochemistry of Peruvian near-surface sediments. *Geochim. Cosmochim. Acta*
503 68, 4429–4451.

504 Borowski, W.S., Rodriguez, N.M., Paull, C.K., Ussler, W., 2013. Are 34S-enriched authigenic
505 sulfide minerals a proxy for elevated methane flux and gas hydrates in the geologic record?
506 *Mar. Pet. Geol.* 43, 381–395.

507 Canfield, D.E., Raiswell, R.R., Westrich, J.T., Reaves, C.M., Berner, R.A., 1986. The use of
508 chromium reduction in the analysis of reduced inorganic sulfur in sediments and shales.
509 *Chem. Geol.* 54, 149–155.

510 Carne, R.C., Cathro, R.J., 1982. Sedimentary exhalative (sedex) zinc-lead-silver deposits,
511 northern Canadian Cordillera. *Can. Min. Metall. Bull.* 75, 66–78.

512 Clarkson, M.O., Poulton, S.W., Guilbaud, R., Wood, R.A., 2014. Assessing the utility of Fe/Al
513 and Fe-speciation to record water column redox conditions in carbonate-rich sediments.
514 *Chem. Geol.* 382, 111–122.

515 Crusius, J., Calvert, S., Pedersen, T., Sage, D., 1996. Rhenium and molybdenum enrichments in
516 sediments as indicators of oxic, suboxic and sulfidic conditions of deposition. *Earth Planet.*
517 *Sci. Lett.* 145, 65–78.

518 Dahl, T.W., Hammarlund, E.U., Anbar, A.D., Bond, D.P.G., Gill, B.C., Gordon, G.W., Knoll,
519 A.H., Nielsen, A.T., Schovsbo, N.H., Canfield, D.E., 2010. Devonian rise in atmospheric
520 oxygen correlated to the radiations of terrestrial plants and large predatory fish. *Proc. Natl.*
521 *Acad. Sci. U.S.A.* 107, 17911–17915.

522 Dellwig, O., Leipe, T., März, C., Glockzin, M., Pollehne, F., Schnetger, B., Yakushev, E. V.,
523 Böttcher, M.E., Brumsack, H.-J., 2010. A new particulate Mn–Fe–P-shuttle at the

1
2
3
4
5
6
7
8
9
10
11
12
13
14
15
16
17
18
19
20
21
22
23
24
25
26
27
28
29
30
31
32
33
34
35
36
37
38
39
40
41
42
43
44
45
46
47
48
49
50
51
52
53
54
55
56
57
58
59
60
61
62
63
64
65

524 redoxcline of anoxic basins. *Geochim. Cosmochim. Acta* 74, 7100–7115.

525 Dickson, A.J., Cohen, A.S., Coe, A.L., 2014. Continental margin molybdenum isotope signatures
526 from the early Eocene. *Earth and Planetary Science Letters*. 404, 389–395.

527 Duan, Y., Anbar, A.D., Arnold, G.L., Lyons, T.W., Gordon, G.W., Kendall, B., 2010.
528 Molybdenum isotope evidence for mild environmental oxygenation before the Great
529 Oxidation Event. *Geochim. Cosmochim. Acta* 74, 6655–6668.

530 Emerson, S.R., Huested, S.S., 1991. Ocean anoxia and the concentrations of molybdenum and
531 vanadium in seawater. *Mar. Chem.* 34, 177–196.

532 Erickson, B.E., Helz, G.R., 2000. Molybdenum(VI) speciation in sulfidic waters: Stability and
533 lability of thiomolybdates. *Geochim. Cosmochim. Acta* 64, 1149–1158.

534 Fallick, A.E., Ashton, J.H., Boyce, A.J., Ellam, R.M., Russell, M.J., 2001. Bacteria were
535 responsible for the magnitude of the world-class hydrothermal base metal sulfide orebody at
536 Navan, Ireland. *Econ. Geol.* 96, 885–890.

537 Fraser, T.A., Hutchison, M.P., 2017. Lithogeochemical characterization of the Middle – Upper
538 Devonian Road River Group and Canol and Imperial formations on Trail River, east
539 Richardson Mountains, Yukon: age constraints and a depositional model for fine-grained
540 strata in the Lower Paleozoic Richardson Trough. *Can. Journ. Earth Sci.* 54, 731–765.

541 Gadd, M.G., Layton-Matthews, D., Peter, J.M., Paradis, S., Jonasson, I.R., 2016. The world-class
542 Howard’s Pass SEDEX Zn-Pb district, Selwyn Basin, Yukon. Part II: the roles of
543 thermochemical and bacterial sulfate reduction in metal fixation. *Miner. Depos.* 1–15.

544 Goldberg, T., Archer, C., Vance, D., Poulton, S.W., 2009. Mo isotope fractionation during
545 adsorption to Fe (oxyhydr)oxides. *Geochim. Cosmochim. Acta* 73, 6502–6516.

546 Goldberg, T., Gordon, G., Izon, G., Archer, C., Pearce, C.R., McManus, J., Anbar, A.D.,
547 Rehkämper, M., 2013. Resolution of inter-laboratory discrepancies in Mo isotope data: an
548 intercalibration. *Journ. Anal. At. Spect.* 28, 724–735.

549 Gomes, M.L., Hurtgen, M.T., 2015. Sulfur isotope fractionation in modern euxinic systems:

1
2
3
4
5
6
7
8
9
10
11
12
13
14
15
16
17
18
19
20
21
22
23
24
25
26
27
28
29
30
31
32
33
34
35
36
37
38
39
40
41
42
43
44
45
46
47
48
49
50
51
52
53
54
55
56
57
58
59
60
61
62
63
64
65

550 Implications for paleoenvironmental reconstructions of paired sulfate–sulfide isotope
551 records. *Geochim. Cosmochim. Acta* 157, 39–55.

552 Goodfellow, W.D., 1987. Anoxic Stratified Oceans as a Source of Sulphur in Sediment-Hosted
553 Stratiform Zn-Pb Deposits (Selwyn Basin, Yukon, Canada). *Chem. Geol. (Isotope Geosci.*
554 *Sect.* 65, 359–382.

555 Goodfellow, W.D., Lydon, J.W., Turner, R.J., 1993. Geology and genesis of stratiform sediment-
556 hosted (SEDEX) zinc-lead-silver sulphide deposits, in: Kirkham, R.W., Sinclair, R., Thorpe,
557 R.I., Duke, J.M. (Eds.), *Mineral Deposit Modeling*. Geological Association of Canada, pp.
558 201–252.

559 Gordey, S.P., Anderson, R.G., 1993. Evolution of the northern cordilleran miogeocline, Nahanni
560 map area (105I), Yukon and Northwest Territories, Memoir 428. ed. Geological Survey of
561 Canada.

562 Gordon, G.W., Lyons, T.W., Arnold, G.L., Roe, J., Sageman, B.B., Anbar, A.D., 2009. When do
563 black shales tell molybdenum isotope tales? *Geology* 37, 535–538.

564 Gromet, L.P., Haskin, L. a., Korotev, R.L., Dymek, R.F., 1984. The “North American shale
565 composite”: Its compilation, major and trace element characteristics. *Geochim. Cosmochim.*
566 *Acta* 48, 2469–2482.

567 Harris, N.B., Mnich, C. a., Selby, D., Korn, D., 2013. Minor and Trace Element and Re-Os
568 Chemistry of the Upper Devonian Woodford Shale, Permian Basin, West Texas: Insights
569 into Metal Abundance and Basin Processes. *Chem. Geol.* 356, 76–93.

570 Horita, J., Zimmerman, H., Holland, H.D., 2002. Chemical evolution of seawater during the
571 Phanerozoic: Implications from the record of marine evaporites. *Geochim. Cosmochim.*
572 *Acta* 66, 3733–3756.

573 House, M.R., 2002. Strength, timing, setting and cause of mid-Palaeozoic extinctions.
574 *Palaeogeog. Palaeoclim. Palaeoeco.* 181, 5–25.

575 Ingall, E.D., Bustin, R.M., Van Cappellen, P., 1993. Influence of water column anoxia on the

1
2
3
4
5
6
7
8
9
10
11
12
13
14
15
16
17
18
19
20
21
22
23
24
25
26
27
28
29
30
31
32
33
34
35
36
37
38
39
40
41
42
43
44
45
46
47
48
49
50
51
52
53
54
55
56
57
58
59
60
61
62
63
64
65

576 burial and preservation of carbon and phosphorus in marine shales. *Geochim. Cosmochim.*
577 *Acta* 57, 303–316.

578 Ingall, E.D., Cappellen, P. Van, 1990. Relation between sedimentation rate and burial of organic
579 phosphorus and organic carbon in marine sediments. *Geochim. Cosmochim. Acta* 54, 373–
580 386.

581 Johnson, C.A., Kelley, K.D., Leach, D.L., 2004. Sulfur and Oxygen Isotopes in Barite Deposits
582 of the Western Brooks Range, Alaska, and Implications for the Origin of the Red Dog
583 Massive Sulfide Deposits. *Econ. Geol.* 99, 1435–1448.

584 Kaufmann, B., 2006. Calibrating the Devonian Time Scale: A synthesis of U-Pb ID-TIMS ages
585 and conodont stratigraphy. *Earth-Science Rev.* 76, 175–190.

586 Lin, Z., Sun, X., Lu, Y., Strauss, H., Xu, L., Gong, J., Teichert, B.M.A., Lu, R., Lu, H., Sun, W.,
587 Peckmann, J., 2016. The enrichment of heavy iron isotopes in authigenic pyrite as a possible
588 indicator of sulfate-driven anaerobic oxidation of methane: Insights from the South China
589 Sea. *Chem. Geol.* 449, 15–29.

590 Lyons, T.W., Gellatly, A.M., Mccgoldrick, P.J., Kah, L.C., 2006. Proterozoic sedimentary
591 exhalative (SEDEX) deposits and links to evolving ocean chemistry. *Geol. Soc. Am. Mem.*
592 198, 169–184.

593 Lyons, T.W., Severmann, S., 2006. A critical look at iron paleoredox proxies: New insights from
594 modern euxinic marine basins. *Geochim. Cosmochim. Acta* 70, 5698–5722.

595 Magnall, J.M., Gleeson, S.A., Paradis, S., 2015. The importance of siliceous radiolarian-bearing
596 mudstones in the formation of sediment-hosted Zn-Pb ± Ba mineralization in the Selwyn
597 Basin, Yukon, Canada. *Econ. Geol.* 110, 2139–2146.

598 Magnall, J.M., Gleeson, S.A., Blamey, N.J.F., Paradis, S., Luo, Y., 2016a. The thermal and
599 chemical evolution of hydrothermal vent fluids in shale hosted massive sulphide (SHMS)
600 systems from the MacMillan Pass district (Yukon, Canada). *Geochim. Cosmochim. Acta*
601 193, 251–273.

1
2
3
4
5
6
7
8
9
10
11
12
13
14
15
16
17
18
19
20
21
22
23
24
25
26
27
28
29
30
31
32
33
34
35
36
37
38
39
40
41
42
43
44
45
46
47
48
49
50
51
52
53
54
55
56
57
58
59
60
61
62
63
64
65

602 Magnall, J.M., Gleeson, S.A., Stern, R.A., Newton, R.J., Poulton, S.W., Paradis, S., 2016b. Open
603 system sulphate reduction in a diagenetic environment – isotopic analysis of barite ($\delta^{34}\text{S}$
604 and $\delta^{18}\text{O}$) and pyrite ($\delta^{34}\text{S}$) from the Tom and Jason Late Devonian Zn-Pb-Ba deposits,
605 Selwyn Basin, Canada. *Geochim. Cosmochim. Acta* 180, 146–163.

606 März, C., Poulton, S.W., Beckmann, B., Küster, K., Wagner, T., Kasten, S., 2008. Redox
607 sensitivity of P cycling during marine black shale formation: Dynamics of sulfidic and
608 anoxic, non-sulfidic bottom waters. *Geochim. Cosmochim. Acta* 72, 3703–3717.

609 McLennan, S., 2001. Relationships between the trace element composition of sedimentary rocks
610 and upper continental crust. *Geochem. Geophys. Geosys.* 2. 2000GC000109.

611 McManus, J., Nägler, T.F., Siebert, C., Wheat, C.G., Hammond, D.E., 2002. Oceanic
612 molybdenum isotope fractionation: Diagenesis and hydrothermal ridge-flank alteration.
613 *Geochemistry, Geophys. Geosystems* 3, 1–9.

614 Morford, J.L., Martin, W.R., Carney, C.M., 2009. Uranium diagenesis in sediments underlying
615 bottom waters with high oxygen content. *Geochim. Cosmochim. Acta* 73, 2920–2937.

616 Nägler, T.F., Siebert, C., Lüschen, H., Böttcher, M.E., 2005. Sedimentary Mo isotope record
617 across the Holocene fresh-brackish water transition of the Black Sea. *Chem. Geol.* 219,
618 283–295.

619 Nägler, T.F., Anbar, A.D., Archer, C., Goldberg, T., Gordon, G.W., Greber, N.D., Siebert, C.,
620 Sohrin, Y., Vance, D., 2014. Proposal for an international molybdenum isotope
621 measurement standard and data representation. *Geostand. and Geoanalyt. Res.* 38, 149–151.

622 Nelson, J., Colpron, M., 2007. Tectonics and metallogeny of the British Columbia, Yukon and
623 Alaskan Cordillera, 1.8 Ga to the present. *Miner. Depos. Canada A Synth. Major Depos.*
624 *Dist. Metallog. Evol. Geol. Prov. Explor. Methods* 2703, 755–791.

625 Neubert, N., Nägler, T.F., Böttcher, M.E., 2008. Sulfidity controls molybdenum isotope
626 fractionation into euxinic sediments: Evidence from the modern Black Sea. *Geology* 36,

1
2
3
4
5
6
7
8
9
10
11
12
13
14
15
16
17
18
19
20
21
22
23
24
25
26
27
28
29
30
31
32
33
34
35
36
37
38
39
40
41
42
43
44
45
46
47
48
49
50
51
52
53
54
55
56
57
58
59
60
61
62
63
64
65

627 775–778.

628 Newton, R.J., Reeves, E.P., Kafousia, N., Wignall, P.B., Bottrell, S.H., Sha, J.-G., 2011. Low
629 marine sulfate concentrations and the isolation of the European epicontinental sea during the
630 Early Jurassic. *Geology* 39, 7–10.

631 Ohmoto, H., Goldhaber, M.B., 1997. Sulfur and Carbon Isotopes, in: Barnes, H.L. (Ed.),
632 *Geochemistry of Hydrothermal Ore Deposits*. John Wiley & Sons, pp. 517–612.

633 Poulson, R.L., Siebert, C., McManus, J., Berelson, W.M., 2006. Authigenic molybdenum isotope
634 signatures in marine sediments. *Geology* 34, 617–620.

635 Poulson Brucker, R.L., McManus, J., Severmann, S., Berelson, W.M., 2009. Molybdenum
636 behavior during early diagenesis: Insights from Mo isotopes. *Geochemistry, Geophys.*
637 *Geosystems* 10, 1–25.

638 Poulton, S., Canfield, D., 2005. Development of a sequential extraction procedure for iron:
639 implications for iron partitioning in continentally derived particulates. *Chem. Geol.* 214,
640 209–221.

641 Poulton, S.W., Canfield, D.E., 2011. Ferruginous Conditions: A Dominant Feature of the Ocean
642 through Earth’s History. *Elements* 7, 107–112.

643 Poulton, S.W., Henkel, S., März, C., Urquhart, H., Flögel, S., Kasten, S., Sinninghe Damsté, J.S.,
644 Wagner, T., 2015. A continental-weathering control on orbitally driven redox-nutrient
645 cycling during Cretaceous Oceanic Anoxic Event 2. *Geology* 43, 963–966.

646 Poulton, S.W., Raiswell, R., 2002. The low-temperature geochemical cycle of iron: from
647 continental fluxes to marine sediment deposition. *Am. J. Sci.* 302, 774–805.

648 Raiswell, R., Canfield, D.E., 1998. Sources of iron for pyrite formation in marine sediments. *Am.*
649 *J. Sci.* 298, 219–245.

650 Redfield, A.C., 1958. The biological control of chemical factors in the environment. *Am. Sci.* 46,
651 205–222.

652 Rempel, K.U., Williams-Jones, A.E., Migdisov, A.A., 2009. The partitioning of molybdenum(VI)

1
2
3
4
5
6
7
8
9
10
11
12
13
14
15
16
17
18
19
20
21
22
23
24
25
26
27
28
29
30
31
32
33
34
35
36
37
38
39
40
41
42
43
44
45
46
47
48
49
50
51
52
53
54
55
56
57
58
59
60
61
62
63
64
65

653 between aqueous liquid and vapour at temperatures up to 370C. *Geochim. Cosmochim.*
654 *Acta* 73, 3381–3392.

655 Reynolds, M.A., Gingras, M.K., Gleeson, S.A., Stemler, J.U., 2015. More than a trace of oxygen:
656 Ichnological constraints on the formation of the giant Zn-Pb-Ag ± Ba deposits, Red Dog
657 district, Alaska. *Geology* 43, 867–870.

658 Scholz, F., Hensen, C., Noffke, A., Rohde, A., Liebetrau, V., Wallmann, K., 2011. Early
659 diagenesis of redox-sensitive trace metals in the Peru upwelling area – response to ENSO-
660 related oxygen fluctuations in the water column. *Geochim. Cosmochim. Acta* 75, 7257–
661 7276.

662 Scholz, F., Löscher, C.R., Fiskal, A., Sommer, S., Hensen, C., Lomnitz, U., Wuttig, K.,
663 Göttlicher, J., Kossel, E., Steininger, R., Canfield, D.E., 2016. Nitrate-dependent iron
664 oxidation limits iron transport in anoxic ocean regions. *Earth Planet. Sci. Lett.* 454, 272–
665 281.

666 Scholz, F., McManus, J., Sommer, S., 2013. The manganese and iron shuttle in a modern euxinic
667 basin and implications for molybdenum cycling at euxinic ocean margins. *Chem. Geol.* 355,
668 56–68.

669 Scholz, F., Severmann, S., McManus, J., Hensen, C., 2014. Beyond the Black Sea paradigm: The
670 sedimentary fingerprint of an open-marine iron shuttle. *Geochim. Cosmochim. Acta* 127,
671 368–380.

672 Scott, C., Lyons, T.W., 2012. Contrasting molybdenum cycling and isotopic properties in euxinic
673 versus non-euxinic sediments and sedimentary rocks: Refining the paleoproxies. *Chem.*
674 *Geol.* 324–325, 19–27.

675 Siebert, C., McManus, J., Bice, A., Poulson, R., Berelson, W.M., 2006. Molybdenum isotope
676 signatures in continental margin marine sediments. *Earth Planet. Sci. Lett.* 241, 723–733.

677 Siebert, C., Nägler, T.F., von Blanckenburg, F., Kramers, J.D., 2003. Molybdenum isotope
678 records as a potential new proxy for paleoceanography. *Earth Planet. Sci. Lett.* 211, 159–

1
2
3
4
5
6
7
8
9
10
11
12
13
14
15
16
17
18
19
20
21
22
23
24
25
26
27
28
29
30
31
32
33
34
35
36
37
38
39
40
41
42
43
44
45
46
47
48
49
50
51
52
53
54
55
56
57
58
59
60
61
62
63
64
65

679 171.

680 Sim, M.S., Ono, S., Hurtgen, M.T., 2015. Sulfur isotope evidence for low and fluctuating sulfate
681 levels in the Late Devonian ocean and the potential link with the mass extinction event.
682 *Earth Planet. Sci. Lett.* 419, 52–62.

683 Slack, J.F., Falck, H., Kelley, K.D., Xue, G.G., 2016. Geochemistry of host rocks in the Howards
684 Pass district, Yukon-Northwest Territories, Canada: implications for sedimentary
685 environments of Zn-Pb and phosphate mineralization. *Miner. Depos.* 52, 565–593.

686 Turner, E.C., Roots, C.F., MacNaughton, R.B., Long, D.G.F., Fischer, B.J., Gordey, S.P., Martel,
687 E., Pope, M.C., 2011. Chapter 3. Stratigraphy, in: Martel, E., Turner, E.C., Fischer, B..
688 (Eds.), *Geology of the Central Mackenzie Mountains of the North Canadian Cordillera,*
689 *Sekwi Mountain (105P), Mount Eduni (106A), and Northwestern Wrigley Lake (95M)*
690 *Map-Areas, Northwest Territories.* NWT Geoscience Office, pp. 31–192.

691 Turner, R.J.W., 1992. Formation of Phanerozoic stratiform sediment , hosted zinc- lead deposits :
692 Evidence for the critical role of ocean anoxia. *Chem. Geol.* 99, 165–188.

693 Tyrrell, T., 1999. The relative influences of nitrogen and phosphorus on oceanic primary
694 production. *Nature* 400, 525–530.

695 Van Cappellen, P., Ingall, E.D., 1994. Benthic phosphorus regeneration, net primary
696 production, and ocean anoxia: A model of the coupled marine biogeochemical cycles of
697 carbon and phosphorus. *Paleoceanography* 9, 677–692.

698 Wheat, C.G., Mottl, M.J., Rudnicki, M., 2002. Trace element and REE composition of a low-
699 temperature ridge-flank hydrothermal spring. *Geochim. Cosmochim. Acta* 66, 3693–3705.

700 Wilkinson, J.J., 2014. Sediment-Hosted Zinc–Lead Mineralization: Processes and Perspectives,
701 in: *Treatise on Geochemistry: Second Edition.* Elsevier Ltd., pp. 219–249.

702

1
2
3
4 703 Figure 1. The paleogeography of North America (Laurentia) during the Late Devonian (380 – 370
5
6 704 Ma). Cross section A – B taken from Nelson and Colpron (2007) and paleogeography
7
8 705 reconstruction annotated from Blakey (2016). The black stars correspond with lithogeochemical
9
10 706 studies conducted on organic-rich mudstones from broadly time equivalent Late Devonian basins:
11
12 707 (1) Selwyn Basin (this study), (2) Western Canadian Sedimentary Basin (Algeo et al., 2007), (3)
13
14 708 Illinois Basin (Dahl et al. 2010), (4) Appalachian Basin (Gordon et al. 2009), (5) Permian Basin
15
16 709 (Harris et al., 2013).

17
18
19
20 710

21
22
23 711 Figure 2. A – The regional extent of the Selwyn Basin in the Canadian Cordillera with the
24
25 712 locations of major sediment hosted massive sulphide deposits (modified from Nelson and
26
27 713 Colpron, 2007). Allochthonous terranes accreted during Mesozoic deformation occur west of the
28
29 714 Tintina Fault; east of this regional structure is the Selwyn Basin and adjoining carbonate platform
30
31 715 that formed a passive margin along the western margin of ancestral North America (Laurentia). B
32
33 716 – A stratigraphic column for the Selwyn Basin, compiled from work mostly conducted at
34
35 717 Macmillan Pass (Abbott and Turner, 1991; Carne and Cathro, 1982; Gordey and Anderson, 1993;
36
37 718 Turner et al., 2011). C – The local geology at Macmillan Pass, along with the location of the
38
39 719 drill-holes from which samples were obtained in this study (modified from Abbott and Turner,
40
41 720 1991).

42
43
44
45
46 721

47
48 722 Figure 3. Lithological sedimentary logs for drill holes TYK-1, 76-17 and TYK-5 with sample
49
50 723 locations annotated by grey arrows. The un-mineralised drill-hole (76-17) has been correlated
51
52 724 with two drill-holes intersecting sulphide mineralisation at the Tom deposit, and is described in
53
54 725 further detail in Magnall et al. (2015). In TYK-1, the vent complex occurs beneath the bedded
55
56 726 mineralisation.

57
58
59
60 727
61
62
63
64
65

1
2
3
4 728 Figure 4. Photographs of un-mineralised mudstone samples from 76-17 and TYK-5, and a sample
5
6 729 of the hydrothermal vent from TYK-1. The areas from which lithochemical analyses were
7
8 730 produced are highlighted by the white boxes and those for thin sections by the red boxes.
9

10
11 731

12
13 732 Figure 5. Lithological logs, Fe speciation (Fe_{PY}/Fe_{HR} and Fe_{HR}/Fe_T) and Mo geochemical data
14
15 733 (abundance and $\delta^{98}Mo$ values) for DH-7617 (A) and DH-TYK5 (B). All samples plot within the
16
17 734 anoxic field ($Fe_{HR}/Fe_T > 0.38$), and samples from TYK-5 contain a higher proportion of pyritised
18
19 735 reactive Fe ($Fe_{PY}/Fe_{HR} > 0.8$). A thick black line represents Late Devonian seawater ($\delta^{98}Mo = 1.5$
20
21 736 ± 0.1 ‰) and the grey dashed line represents Mo enrichment in euxinic settings (Scott and Lyons,
22
23 737 2012).
24

25
26 738

27
28
29 739 Figure 6. A – histogram of Fe/Al for mudstones from DH-76-17 and DH-TYK-5, compared with
30
31 740 mudstones from the Richardson Trough (Fraser and Hutchison, 2017). B – Fe_{PY}/Fe_{HR} vs. $\delta^{34}S$
32
33 741 values (Magnall et al. 2016b) in samples from 76-17 (hollow) and TYK-5 (solid).
34

35
36 742

37
38 743 Figure 7. Box and whisker plots for Pb, Zn and Mo in mudstone samples from 76-17 (grey),
39
40 744 TYK-5 (black) and the mineralised vent (orange). Circles and lines denote the median and
41
42 745 average, respectively, and whiskers extend to outliers beyond the 1st and 3rd quartiles.
43

44
45 746

46
47 747 Figure 8. TOC vs. Mo (ppm) for samples from Macmillan Pass (this study) and the Richardson
48
49 748 Trough (Fraser and Hutchison, 2017).
50

51
52 749

53
54 750

55
56 751 Figure 9. A – Log TOC/P (molar ratio) vs. Log Mo_{EF} for Macmillan Pass mudstones and
57
58 752 Richardson Trough samples. Box and whisker plots for the sample sub-groups are included at the
59
60

61
62
63
64
65

1
2
3
4 753 top of the figure (note the different axis), with boxes representing the interquartile range, white
5
6 754 circles the average and outliers ($1.5 * Q3 - Q1$) data that plots beyond the whiskers. B – Log
7
8 755 TOC/P (molar ratio) vs. Log P/Al (wt. %) for Macmillan Pass mudstones and Richardson Trough
9
10 756 samples. Separate regression lines (dotted) are plotted for Macmillan Pass and Richardson
11
12 757 Trough samples, and also for the combined data set (solid).

13
14
15 758

16
17 759 Figure 10. Chronostratigraphy of the Late Devonian with annotated conodont biostratigraphy
18
19 760 (Kaufmann, 2006), mass extinction events (House, 2002) and published $\delta^{98}\text{Mo}$ values (this study;
20
21 761 Gordon et al., 2009; Dahl et al. 2010). The isotopic fractionation of Mo between Late Devonian
22
23 762 seawater ($\delta^{98}\text{Mo} = 1.5 \pm 0.1 \text{‰}$) and sediment deposited in contrasting redox environments
24
25 763 ($\Delta^{98}\text{Mo}_{\text{SW-SED}}$): euxinic (Neubert et al., 2008), anoxic (Poulson et al., 2006; Poulson Brucker et
26
27 764 al., 2009), suboxic and oxic (Siebert et al., 2006), and the suggested $\delta^{98}\text{Mo}$ value for low-
28
29 765 temperature hydrothermal fluids (McManus et al., 2002).

30
31
32 766

33
34 767 Figure 11. The abundance of Mo and U for Macmillan Pass and Richardson Trough mudstones
35
36 768 calculated as enrichment factors ($X_{\text{EF}} = (X/\text{Al})_{\text{sample}} / (X/\text{Al})_{\text{NASC}}$), where NASC = North American
37
38 769 Shale Composite (Gromet et al., 1984). The annotated redox states (suboxic, anoxic and euxinic)
39
40 770 correspond with the observation that relative to seawater (sw), Mo enrichment exceeds U
41
42 771 enrichment in progressively reducing conditions; however, more extreme enrichment of Mo over
43
44 772 U also occurs during particulate shuttling of Fe-Mn oxyhydr(oxides), when these complexes are
45
46 773 deposited and subsequently dissolved during early diagenesis (Algeo and Tribovillard, 2009).

47
48
49 774

50
51
52 775 Figure 12. A – $\delta^{98}\text{Mo}$ vs. Fe/Al for Macmillan Pass mudstones. Samples with low Fe/Al (< 0.44)
53
54 776 preserve a good correlation ($r^2 = 0.82$) between $\delta^{98}\text{Mo}$ and Fe/Al. Samples located within 15
55
56 777 meters of the mineralised interval in DH-TYK-5 form another sub-group, as they preserve

1
2
3
4
5
6
7
8
9
10
11
12
13
14
15
16
17
18
19
20
21
22
23
24
25
26
27
28
29
30
31
32
33
34
35
36
37
38
39
40
41
42
43
44
45
46
47
48
49
50
51
52
53
54
55
56
57
58
59
60
61
62
63
64
65

778 evidence of post depositional pyrite enrichment and phyllosilicate alteration associated with the
779 hydrothermal system (described in Magnall et al. 2015). B – closed system Rayleigh fractionation
780 model describing the evolution of $\delta^{98}\text{Mo}_{\text{fluid}}$ values that occurs with progressive complexation of
781 Mo to Fe (oxyhydr)oxides. The upper and lower dotted lines represent goethite and ferrihydrite
782 respectively; the solid line represents a fractionation factor intermediate between the two.

Figure1
[Click here to download high resolution image](#)

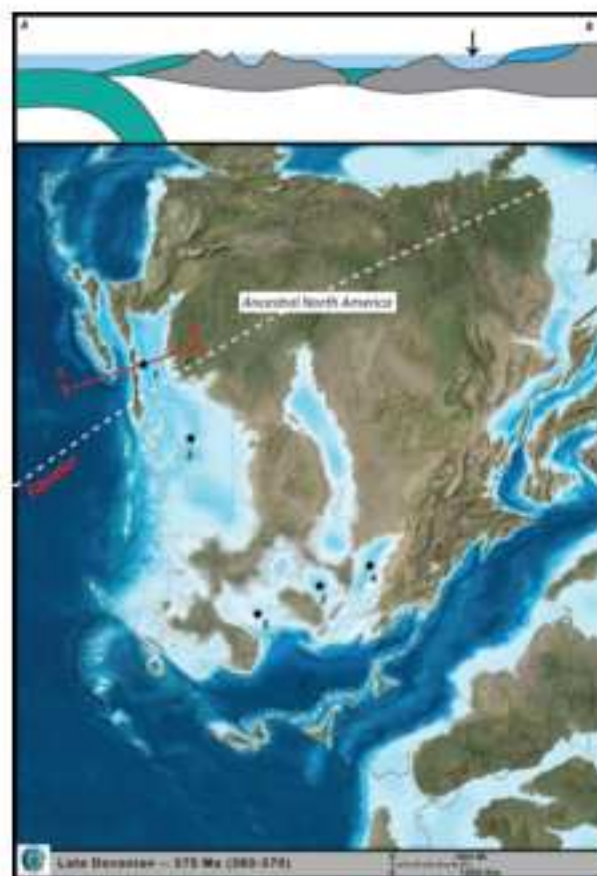


Figure2
[Click here to download high resolution image](#)

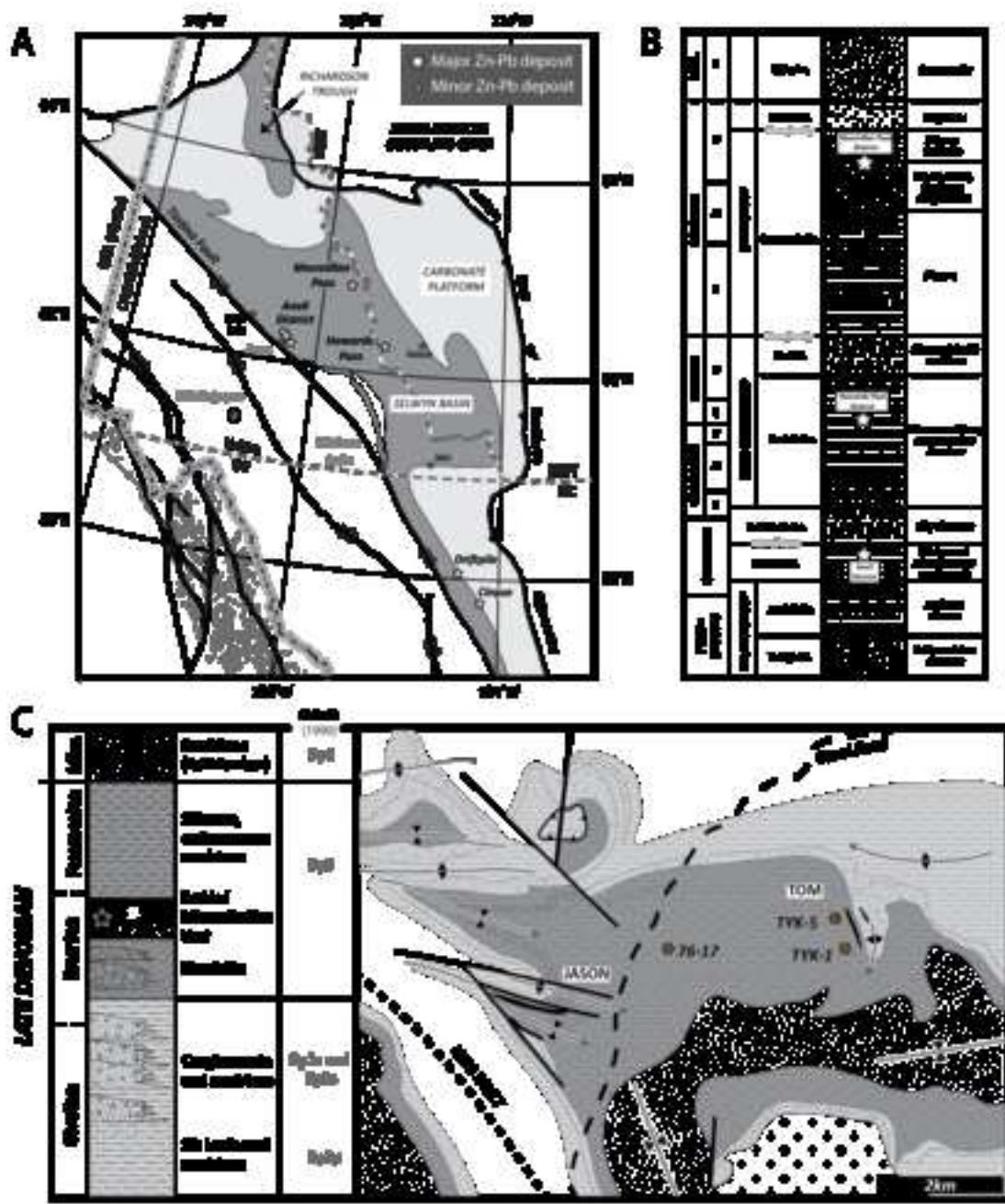


Figure3
[Click here to download high resolution image](#)

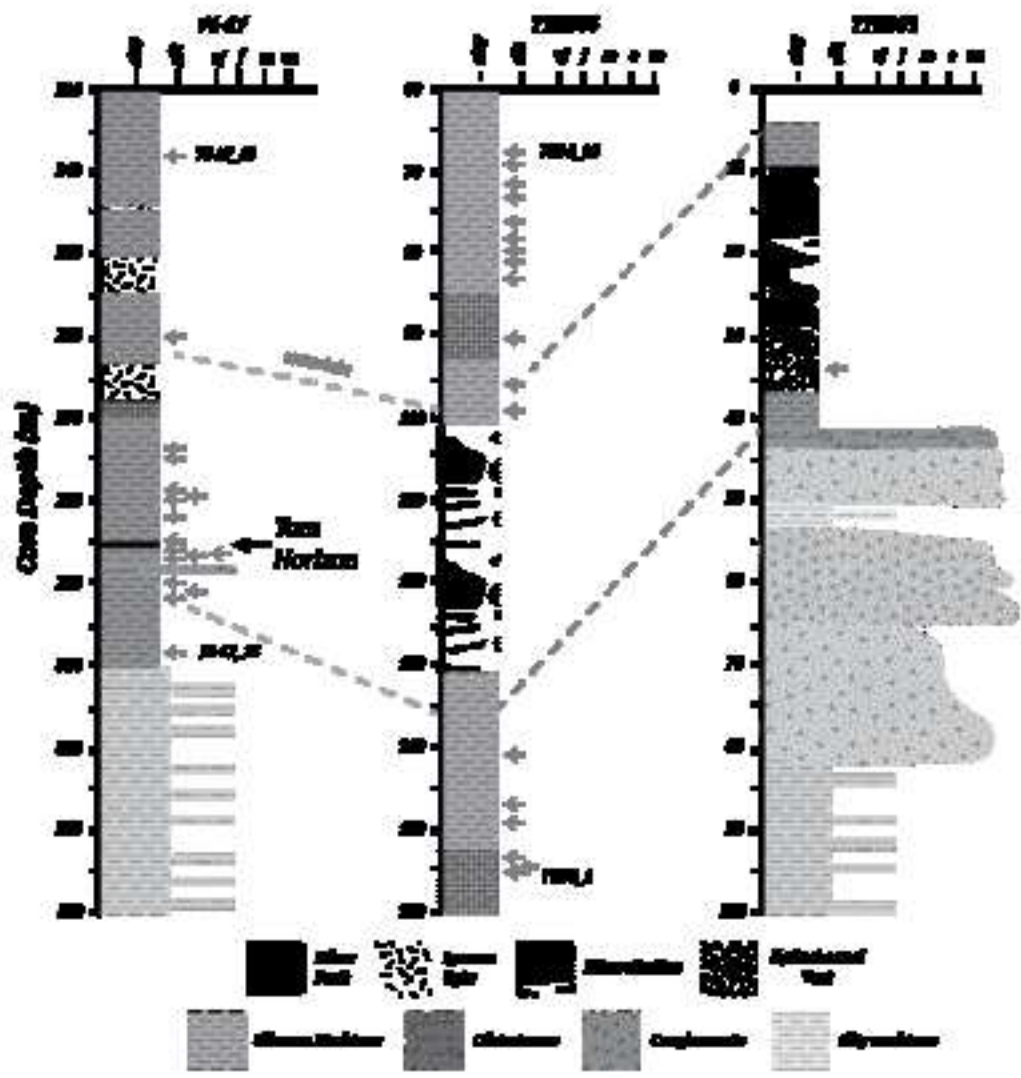


Figure 5
[Click here to download high resolution image](#)

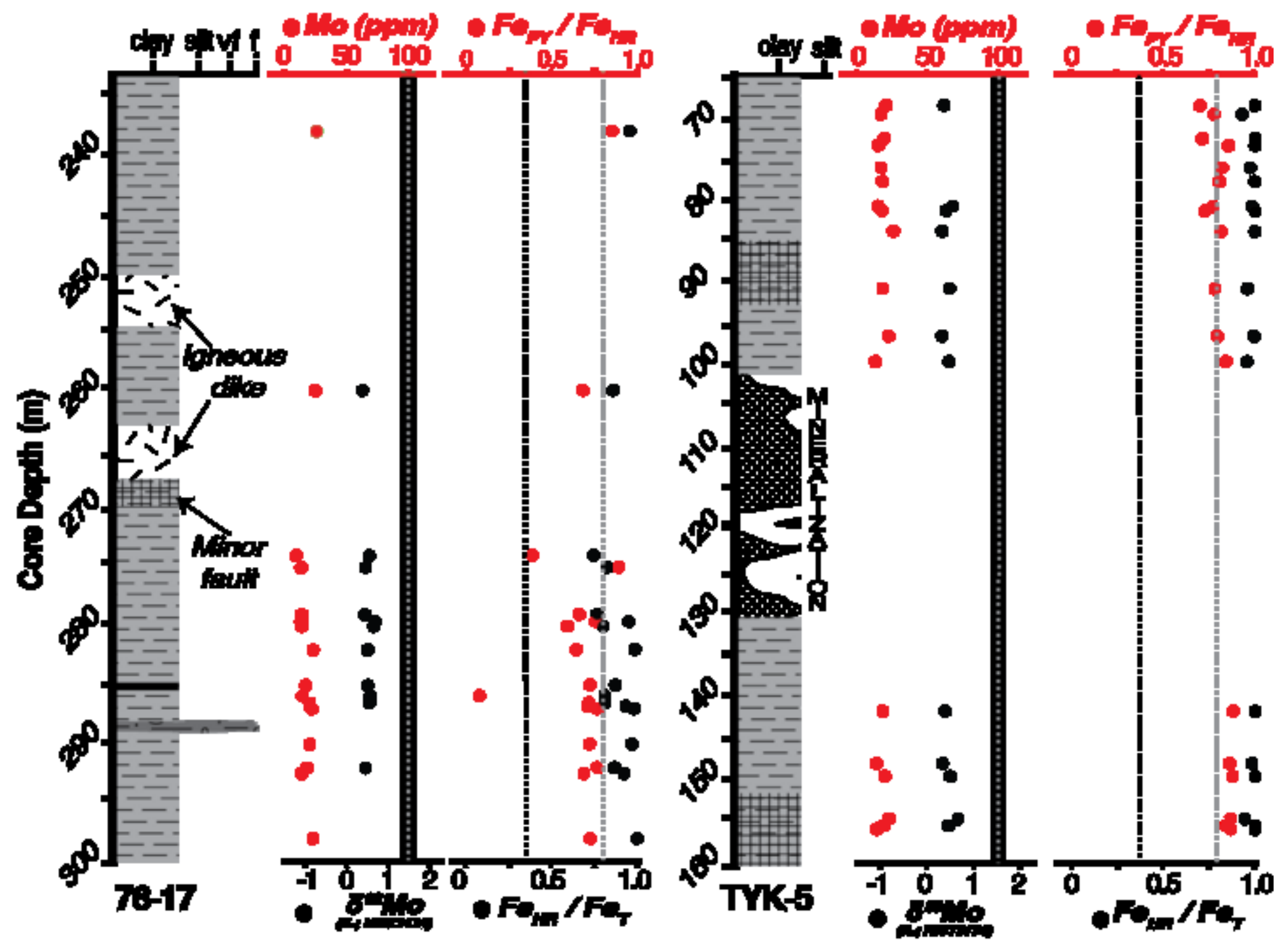


Figure 6

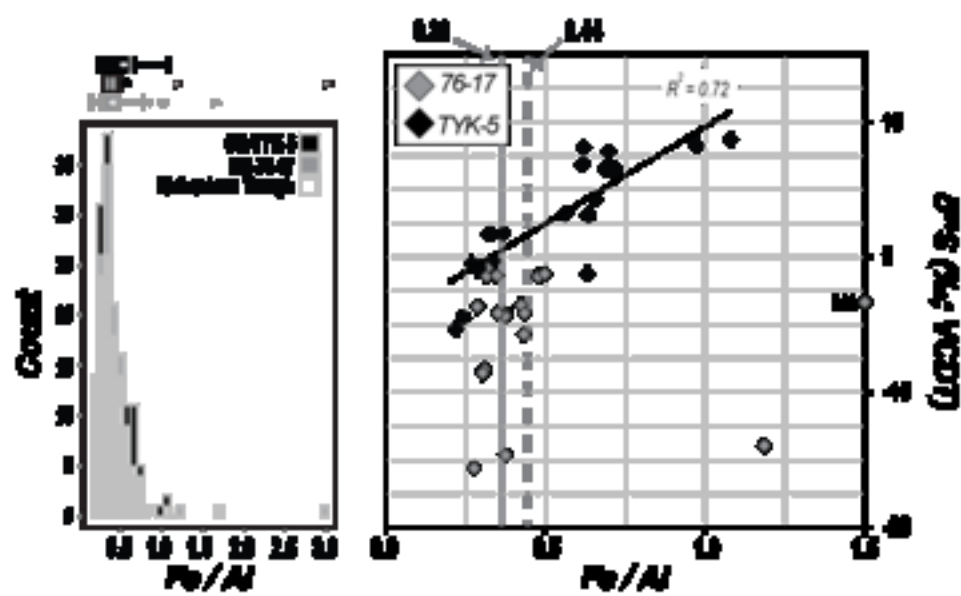


Figure 6

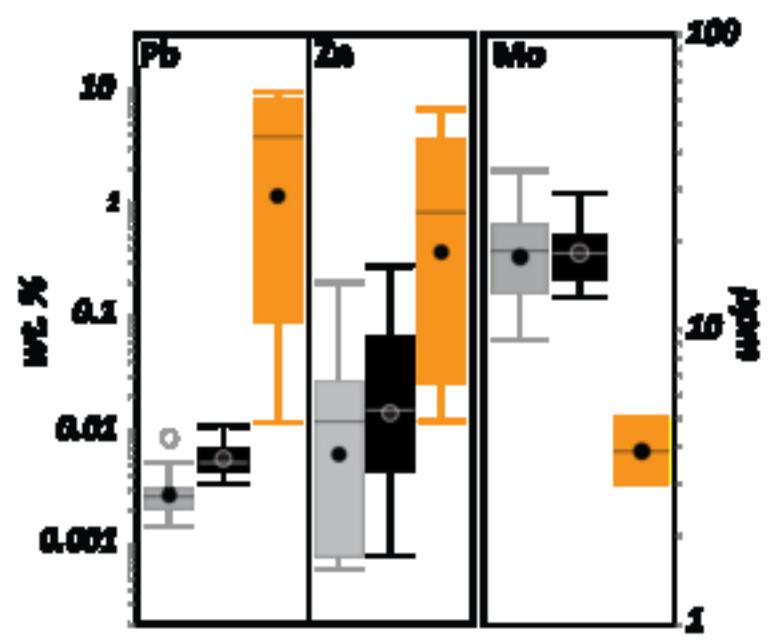


Figure 8

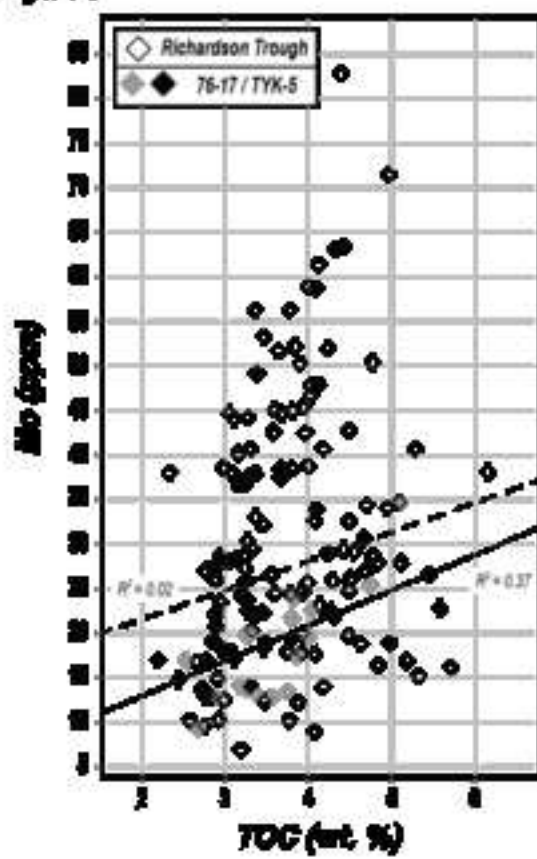


Figure 9

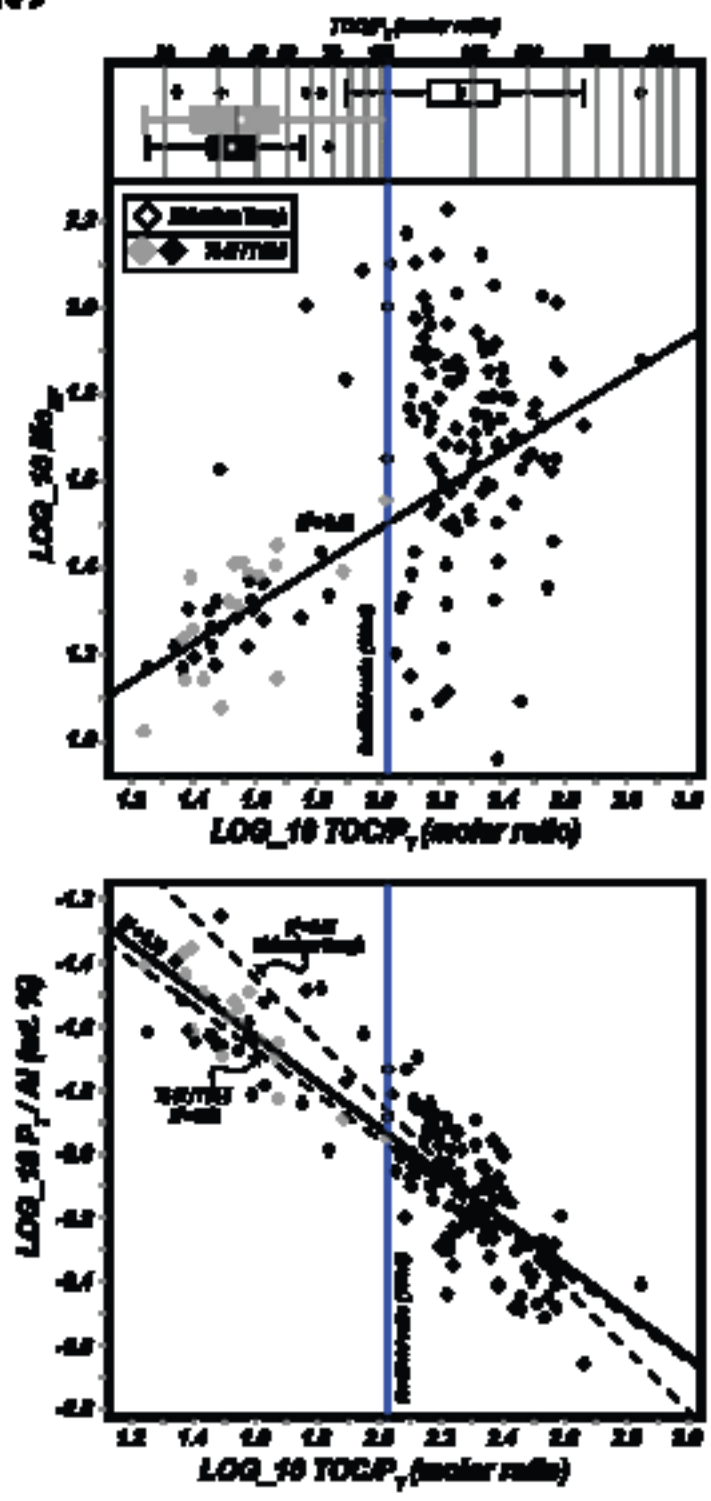


Figure 10

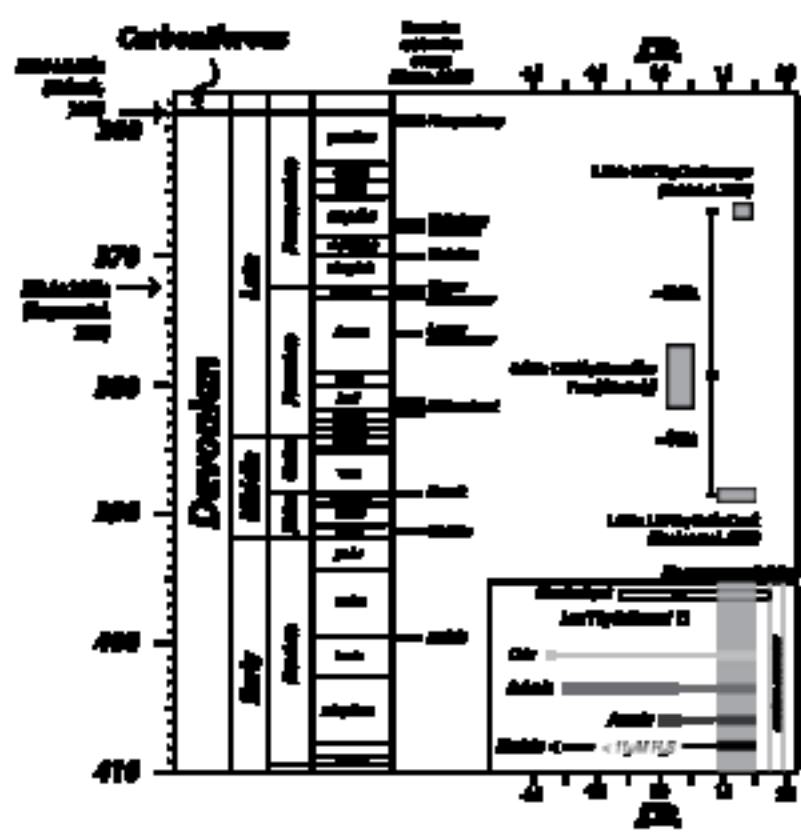
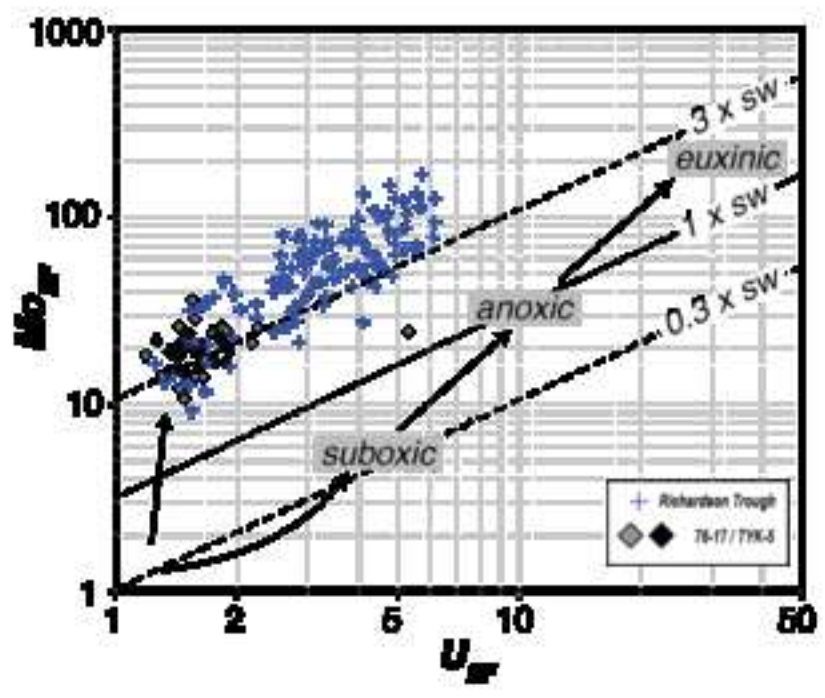


Figure 11



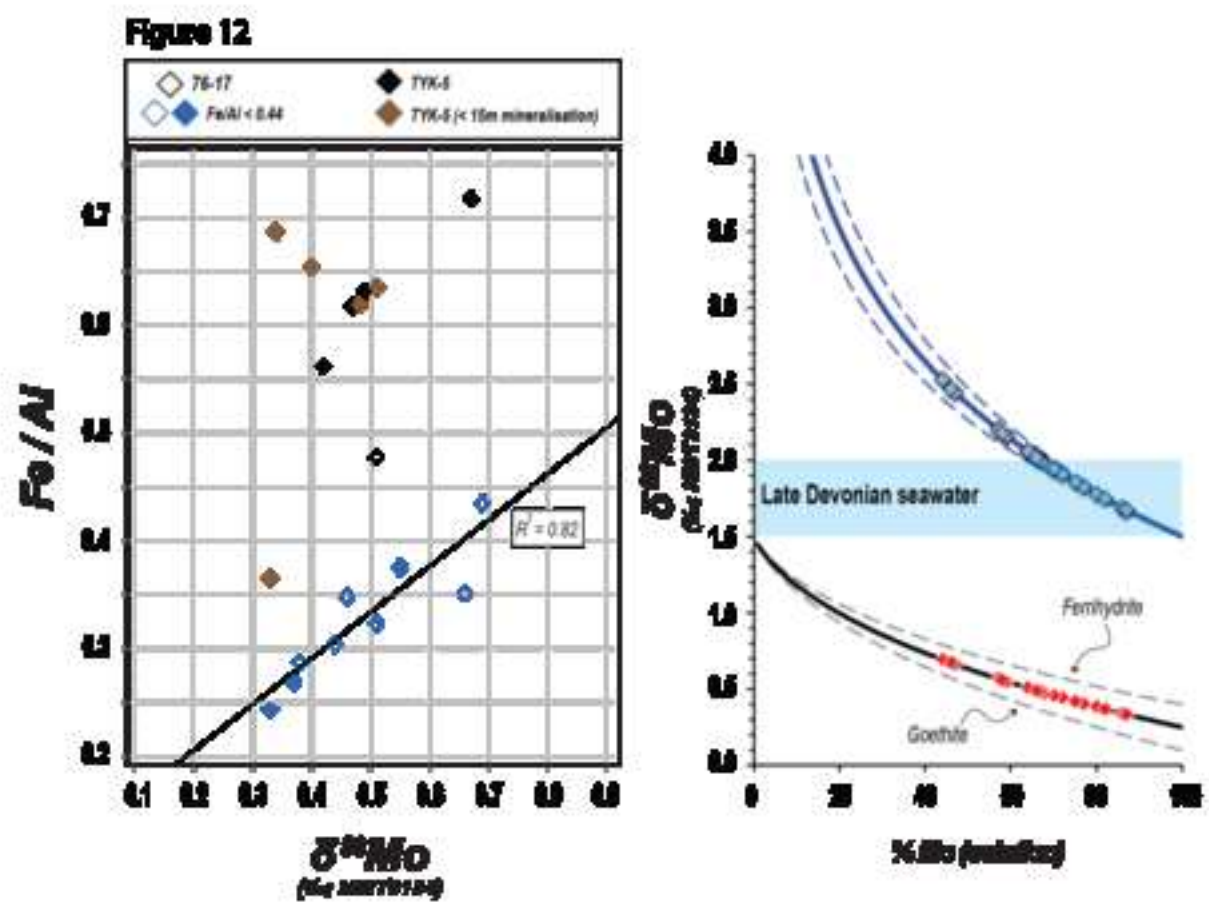


Table1

[Click here to download Table: Table1.xlsx](#)

Sample #	Metres	C _{org}	P	S _T	Al _T	Fe _T	Pb	Zn	Mo	U	Mo _{EF}	U _{EF}
		wt. %						ppm				
76-17_15	298	4.0	0.1	1.1	3.9	1.7	43.0	227.0	22.5	6.1	25.6	2.2
76-17_17	292.5	3.4	0.1	0.8	3.4	1.1	26.5	587.0	13.1	3.9	17.2	1.7
76-17_18	292	3.9	0.1	1.1	3.8	1.3	29.7	276.0	17.5	4.9	20.5	1.8
76-17_20	290	3.3	0.1	1.2	3.5	1.5	30.9	226.0	19.9	4.4	25.6	1.8
76-17_22	287	3.8	0.1	1.3	4.0	1.5	29.8	521.0	21.7	5.3	23.9	1.9
76-17_23	286.8	4.0	0.2	0.9	3.6	1.1	20.4	173.0	19.6	4.4	23.9	1.7
76-17_24	286.5	3.3	0.1	0.9	3.1	1.2	21.6	271.0	19.9	3.4	28.4	1.6
76-17_26	285.9	3.2	0.1	0.7	2.6	7.7	14.3	149.0	14.1	9.5	24.4	5.3
76-17_29	285	2.5	0.1	1.0	4.1	1.3	21.5	98.0	16.9	3.4	18.2	1.2
76-17_31	282	4.0	0.1	1.5	4.1	1.9	30.7	1999.0	22.6	5.3	24.7	1.9
76-17_32	280	3.3	0.1	1.1	5.1	1.8	25.1	15.0	13.8	5.1	12.0	1.4
76-17_33	279.6	3.6	0.1	1.4	4.1	1.8	26.7	10.0	12.9	4.7	13.9	1.6
76-17_34	279	3.7	0.2	1.0	4.3	1.3	21.6	7.0	13.5	4.7	13.9	1.6
76-17_35	275	2.9	0.1	5.1	4.1	4.8	86.4	7.0	12.9	3.7	14.0	1.3
76-17_36	274	2.7	0.2	0.8	3.9	1.5	15.7	8.0	9.3	4.0	10.6	1.5
76-17_38	260	3.8	0.1	0.9	4.1	1.2	16.8	6.0	24.0	4.1	25.9	1.4
76-17_40	238	4.7	0.1	2.6	5.4	2.7	53.3	8.0	25.4	8.1	21.1	2.2
76-17_41	225	5.1	0.0	0.8	4.3	1.2	29.1	12.0	34.6	4.6	35.9	1.5
<i>median</i>		3.7	0.1	1.0	4.1	1.5	26.6	123.5	18.6	4.7	22.5	1.6
<i>min</i>		2.5	0.0	0.7	2.6	1.1	14.3	6.0	9.3	3.4	10.6	1.2
<i>max</i>		5.1	0.2	5.1	5.4	7.7	86.4	1999.0	34.6	9.5	35.9	5.3
TYK5-1	155.4	3.3	0.1	4.3	3.7	4.0	89.9	190.0	14.0	4.6	16.6	1.8
TYK5-2	155	5.0	0.1	3.3	5.1	3.1	105.1	86.0	18.9	6.6	16.6	1.9
TYK5-3	154.18	5.6	0.1	3.5	4.4	3.1	79.5	25.0	22.8	5.4	23.2	1.8
TYK5-6	149.08	3.8	0.1	3.0	4.3	2.7	69.9	15.0	19.5	5.6	20.1	1.9
TYK5-7	147.54	2.7	0.1	3.0	4.1	2.8	58.6	8.0	13.7	4.5	15.0	1.6
TYK5-8	141.29	3.5	0.1	3.0	4.2	2.8	52.7	11.0	18.4	5.6	19.3	1.9
TYK5-10	99.41	2.8	0.1	2.4	3.9	2.4	110.2	258.0	12.9	4.0	14.8	1.5
TYK5-11	96.37	2.9	0.1	2.0	4.9	1.8	48.6	1241.0	22.1	5.5	20.2	1.6
TYK5-12	90.66	3.0	0.1	2.6	4.2	2.7	64.5	152.0	18.2	4.0	19.0	1.3
TYK5-13	83.84	3.2	0.1	1.4	5.4	1.3	44.3	678.0	25.8	5.5	21.2	1.5
TYK5-14	81.36	3.0	0.1	1.7	3.3	1.9	50.6	264.0	17.6	3.5	23.5	1.5
TYK5-14A	80.82	2.4	0.1	3.1	3.6	3.5	48.8	70.0	14.8	3.6	18.3	1.4
TYK5-15	77.82	3.1	0.1	2.7	4.1	2.9	66.3	71.0	18.0	4.5	19.3	1.6
TYK5-16	76.19	2.2	0.1	1.7	5.1	1.7	49.2	112.0	17.0	4.8	14.9	1.4
TYK5-17	73.52	2.5	0.1	1.4	4.2	1.4	43.2	249.0	14.9	4.2	15.6	1.4
TYK5-18	72.7	2.9	0.1	1.2	4.3	1.2	33.9	1751.0	19.2	4.2	20.0	1.4
TYK5-19	69.81	2.8	0.1	1.1	4.1	1.2	36.4	692.0	16.9	3.9	18.5	1.4
TYK5-20	68.72	2.9	0.1	1.2	4.4	1.2	38.6	2798.0	20.7	4.5	21.1	1.5
TYK5-21	29.33	4.2	0.1	1.3	5.9	1.3	54.8	45.0	29.0	5.2	21.7	1.3
<i>median</i>		3.0	0.1	2.4	4.2	2.4	52.7	152.0	18.2	4.5	19.3	1.5
<i>min</i>		2.2	0.1	1.1	3.3	1.2	33.9	8.0	12.9	3.5	14.8	1.3
<i>max</i>		5.6	0.1	4.3	5.9	4.0	110.2	2798.0	29.0	6.6	23.5	1.9
Vent		wt. %										
T91.14-11		0.0	5.0	0.6	20.8	0.7	0.0	5.0	1.2			
TYK1-6		0.1	1.9	0.7	26.4	0.0	0.1	3.0	0.7			
TYK2-14		0.0	30.6	0.7	2.0	7.1	0.8	<DL	0.5			
TYK2-15		0.0	8.3	0.5	25.9	9.4	1.9	<DL	0.4			
TYK2-17		<DL	24.7	0.5	17.5	3.8	6.7	<DL	0.3			

Table2

[Click here to download Table: Table2.xlsx](#)

Sample #	Metres	Fe _{mag}	Fe _{ox}	wt. %			Fe _{py} / Fe _{tot}	Fe _{hr} / Fe _T	δ ⁵⁶ Mo (‰)				δ ³⁴ S (‰)	
				Fe _{carb}	Fe _{py}	Fe _{hr}			RochMo2	Nist3134	2σ	n		
76-17_15	298	0.02	0.05	0.55	1.65	2.26	0.73	1.34						-5.7
76-17_17	292.5	0.01	0.06	0.16	0.68	0.91	0.74	0.85						-1.4
76-17_18	292	<DL	0.04	0.20	0.88	1.12	0.78	0.85	0.79	0.48	0.01	3		-1.3
76-17_20	290	<DL	0.05	0.34	1.03	1.42	0.72	0.97						-3.5
76-17_22	287	<DL	0.04	0.24	1.14	1.42	0.80	0.94						-4.2
76-17_23	286.8	<DL	0.03	0.24	0.75	1.01	0.74	0.90						-8.3
76-17_24	286.5	<DL	0.04	0.23	0.68	0.95	0.72	0.81	0.88	0.57	0.03	3		-4.3
76-17_26	285.9	1.38	1.21	3.19	0.50	6.27	0.08	0.81	0.90	0.59	0.02	3		-3.2
76-17_29	285	<DL	0.07	0.25	0.84	1.17	0.72	0.87	0.84	0.53	0.05	3		-0.7
76-17_31	282	0.01	0.07	0.45	1.24	1.77	0.70	0.91	0.84	0.53	0.01	3		-1.4
76-17_32	280	0.02	0.04	0.47	0.85	1.44	0.59	0.80	0.99	0.68	0.01	3		-4.1
76-17_33	279.6	0.05	0.10	0.26	1.29	1.70	0.76	0.95	1.02	0.71	0.04	3		-4.1
76-17_34	279	0.03	0.06	0.25	0.66	1.00	0.66	0.77	0.77	0.46	0.03	3		-8.6
76-17_35	275	0.03	0.14	0.26	3.54	3.98	0.89	0.82	0.79	0.48	0.05	3		-13.9
76-17_36	274	0.06	0.11	0.50	0.43	1.10	0.39	0.75	0.88	0.57	0.06	3		-14.6
76-17_38	260	0.03	0.08	0.22	0.69	1.01	0.68	0.86	0.71	0.40	0.05	3		-3.6
76-17_40	238	0.02	0.06	0.30	2.18	2.55	0.85	0.96						-1.2
76-17_41	225	0.02	0.10	0.31	0.60	1.03	0.58	0.87						-15.6
<i>median</i>		0.02	0.06	0.26	0.85	1.29	0.72	0.86	0.84	0.53				-4.1
<i>min</i>		0.01	0.03	0.16	0.43	0.91	0.08	0.75	0.71	0.40				-15.6
<i>max</i>		1.38	1.21	3.19	3.54	6.27	0.89	1.34	1.02	0.71				-0.7
TYK5-1	155.4	0.1	0.1	0.4	3.6	4.1	0.87	1.02						8.7
TYK5-2	155	0.1	0.1	0.4	2.7	3.2	0.85	1.02	0.80	0.49	0.10	4		6.9
TYK5-3	154.18	0.0	0.1	0.3	2.6	3.0	0.87	0.95	1.00	0.69	0.02	3		6.5
TYK5-6	149.08	0.0	0.1	0.3	2.6	2.9	0.88	1.06	0.84	0.53	0.05	3		3.1
TYK5-7	147.54	0.0	0.1	0.3	2.4	2.8	0.87	0.99	0.67	0.36	0.05	3		6.5
TYK5-8	141.29	0.0	0.1	0.2	2.5	2.8	0.89	1.01	0.73	0.42	0.03	3		4.3
TYK5-10	99.41	0.0	0.1	0.3	2.0	2.3	0.85	0.96	0.81	0.50	0.09	4		8.1
TYK5-11	96.37	0.0	0.0	0.2	1.4	1.7	0.84	0.95	0.66	0.35	0.06	3		1.7
TYK5-12	90.66	0.0	0.1	0.5	2.0	2.6	0.79	0.96	0.82	0.51	0.04	3		-1.2
TYK5-13	83.84	0.0	0.0	0.1	1.1	1.3	0.85	0.97	0.66	0.35	0.11	3		-4.4
TYK5-14	81.36	0.0	0.1	0.4	1.4	1.9	0.74	1.02	0.75	0.44	0.07	5		3.2
TYK5-14A	80.82	0.0	0.0	0.7	2.7	3.5	0.78	0.99	0.89	0.58	0.03	3		8.3
TYK5-15	77.82	0.0	0.0	0.6	2.7	3.4	0.81	1.16						7.8
TYK5-16	76.19	0.0	0.0	0.2	1.4	1.7	0.82	0.98						-0.3
TYK5-17	73.52	0.0	0.0	0.1	1.4	1.6	0.86	1.17						1.7
TYK5-18	72.7	0.0	0.0	0.2	0.9	1.2	0.78	0.93						-0.8
TYK5-19	69.81	0.0	0.0	0.2	0.9	1.1	0.79	0.92						-0.7
TYK5-20	68.72	0.0	0.0	0.1	0.9	1.1	0.85	0.93	0.70	0.39	0.08	4		-0.5
TYK5-21	29.33	0.0	0.0	0.2	0.8	1.0	0.78	0.73						-5.3
<i>median</i>		0.02	0.05	0.26	1.96	2.31	0.85	0.98	0.78	0.46				3.09
<i>min</i>		0.01	0.03	0.13	0.75	0.96	0.74	0.73	0.66	0.35				-5.27
<i>max</i>		0.10	0.07	0.71	3.59	4.11	0.89	1.17	1.00	0.69				8.71
SDO-1									1.11	0.80	0.06	11		
KyotoMo									-0.06	-0.37	0.04	11		
ImperialMo									0.15	-0.16	0.05	10		